UNIVERSITÀ DEGLI STUDI DI PADOVA

FACOLTÀ DI INGEGNERIA

CORSO DI LAUREA MAGISTRALE IN BIOINGEGNERIA

A GLOBAL TORTUOSITY MEASURE FOR THE RETINAL VASCULATURE: DEFINITION AND TESTS WITH A REAL CLINICAL DATA SET

GIORGIA PREVEDELLO

SUPERVISOR	PROFESSOR ENRICO GRISAN
CO-SUPERVISOR	PROFESSOR EMANUELE TRUCCO

PADOVA, 23 APRILE 2013

ACKNOWLEDGEMENTS

I would like to express my deep gratitude to Professor Emanuel Trucco, my research supervisor, for his help and enthusiastic encouragement during my research work. My grateful thanks are to Dr. Diego Gadelha for his patient guidance and precious assistance with the data set annotations. I would also like to extend my thanks to Kris Zutis for his help in running the classification tests, the VAMPIRE team and Professor Enrico Grisan for their willingness.

I'm also grateful to my parents and my family for their love, support and encouragement throughout my studies and above all for all the opportunities they gave me.

Finally I wish to thank all the people I met in Scotland for making me feel home and for have been part of an amazing experience; my heartiest thanks to all my friends for the love, the laughs and for always being there for me.

INDEX

LIST OF FIGURES

LIST OF TABLES

ABSTRACT

Tortuosity is a concept that aims to quantify the amount of bending of blood vessels: the more a vessel is bent and tormented, the higher the tortuosity is. Clinicians rely on experience and examples for tortuosity assessment, so a quantitative model of tortuosity allows a repeatable and automatic computation, and overcomes the variability of clinical judgment.

The purpose of this research work is to evaluate whether it is possible to obtain a consistent quantification of the tortuosity of the retinal vessels by mean of the spectral analysis. State of art models are based on local properties, computed at each point of the blood vessels; the advantage of a spectral model is to offer a description of the tortuosity considering the vessel in its entirety. Moreover, starting from the information acquired for each vessel, it has been tried to provide a global assessment of tortuosity for the full vascular network.

The idea behind a model based on the spectral analysis is being able to classify images according to an overall level of tortuosity rather than classify single segment or vessel. In order to achieve these results test have been run on a dataset of images recorded at clinic of Hospital das Clínicas da Universidade Federal de Pernambuco; moreover the our model does not learn any parameter form examples or other tests.

Generally a single vessel is defined as the continuous vascular segment between two breaking points, in this experimental study in order to compute the spectral analysis on the longest possible vessel it has been decided to trace manually the vascular network according to a well-defined criterion. Main arteries and veins have been traced starting from the optic disc until the end of the field of view, while secondary vessels have been traced starting from the branching points along principal vessels.

Once the profile of the vascular network has been delineated each image has been processed: at first analyzing single vessels then assessing a tortuosity measure for the entire image. Eventually, in order to verify the goodness and the validity of the technique, the outcomes have been used to test whether the spectral model follows medical judgments and ophthalmologists classifications and whether it can be considered a reliable tool for automatic computation both for vessels and images tortuosity.

CHAPTER 1: INTRODUCTION

1.1 ANATOMY OF THE HUMAN EYE

The human eye is a slightly asymmetric globe with the diameter of about 24 millimeters; it is enveloped by three layers: the outermost the sclera, which is the external protection of the ocular globe and in its anterior part, modified to form the cornea; as second and third inner layers we find the choroid and the retina.

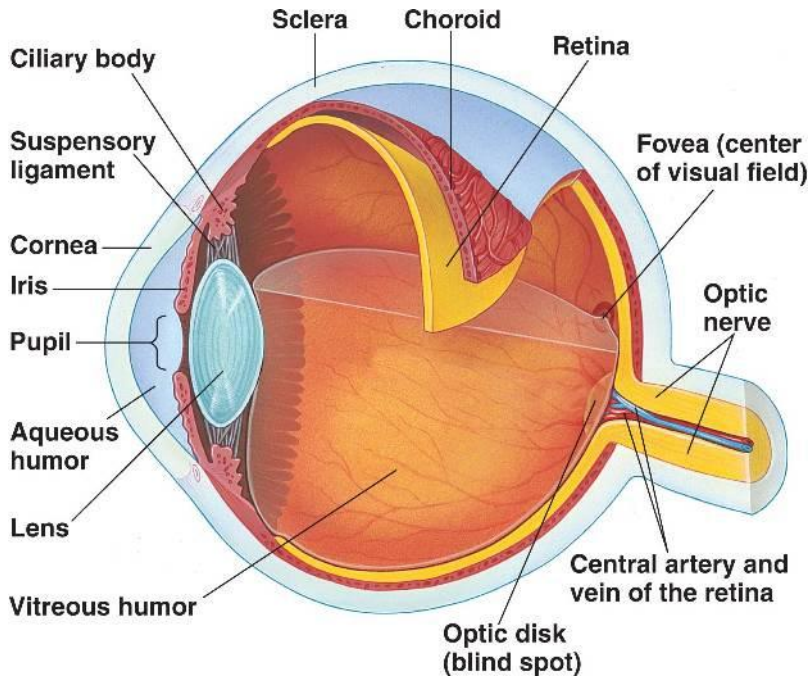

Figure 1.1: Eye Structure

In the anterior part of the eye, right behind the cornea, it is located the iris, the pigmented part which contains muscle fibers to control the movements of the pupil; the pupil is a black circular opening of the iris that lets the light in. Behind the iris lays the lens which helps focusing the light on the back of the eye. Between the lens and the rear part of the globe there is a clear gel called vitreous.

In the back of the eye, we found the retina, which is a layered structure composed of several layer of neurons connected by synapses. There are two types of neurons in the retina, photoreceptors cells called rods and cones, these neurons convert the light into electrical impulses. Rods function mainly in dim light and provide black and white vision, while cones support day time vision and perception of colors.

At the end of the neuronal path ganglion cells convert the signals into action potentials, and then through their axons, the signals reach the optic nerve and the brain. There are two sources of blood supply to the retina: the central retinal artery and the choroidal blood vessels. The choroid receives the greatest blood flow and it is vital for the maintenance of the outer part of the retina, specially the photoreceptors, the remaining blood flow reaches the retina through the central retinal artery and nourishes the inner retinal layer. The arterial intraretinal branches supply three layers of capillary networks: the radial peripapillary capillaries and an inner and outer layer of capillaries. The peripapillary venules drain into venules and through the corresponding venous system to the central retinal vein. The outermost arterioles and venules are the ones detected by ophthalmoscopy and fundus photography and

Both optic nerve and blood vessels leave the eye through the optic disc, which is located in the nasal area of the retina and called “blind spot” because it leaks of photoreceptors. Opposite to the optic disc, on the temporal area, it is located the macula, at its center the foveal pit is a small region rich in cones and poor in rods and with no blood vessels. The fovea is the region of the retina where the visual acuity reaches the maximum and when we focus our attention on a specific object our eyes move in order that the light rays coming from the object hit the fovea.

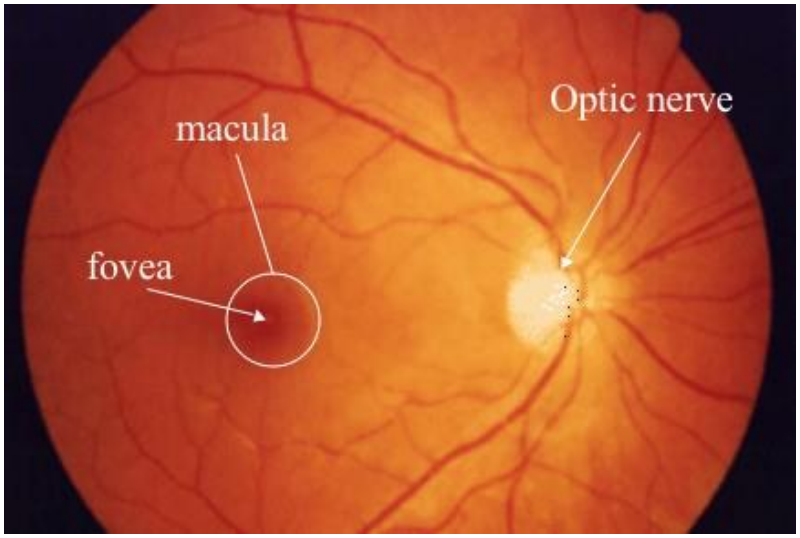

Figure 1.2: Retina Landmarks: fovea, macula and optic nerve

1.2 RETINAL DISEASES AND SYSTEMIC DISEASES WITH RETINAL MANIFESTATION

Through retinal images analysis it is possible to detect many disease that manifest themselves in the retina and originate in the eye, the brain or the cardiovascular system. Hereafter an overview of the most prevalent disease studied via eye imaging:

- *Diabetes*, diabetes mellitus is typically diagnosed in subjects with fasting plasma glucose over 7.0 mmol/l; one of the complications of diabetes mellitus in the eye is known as *Diabetic Retinopathy*. Hyperglycemia is known for damaging small and large blood vessels; its effects can be seen in the retina vasculature network where it damages the retinal vessel walls causing *ischemia* (resulting in the growth of new blood vessels) and *breakdown of the blood-retinal barrier* (leading to fluid leakage, diabetic macular edema and damage to photoreceptors).

- *Age-related macular degeneration*, which manifest itself in two major forms: wet and dry. Dry age-related macular degeneration leads to gradual loss of visual acuity while wet one is characterized by ingrowth of choroidal vascular structure into the macula along with increased vascular permeability. The increase of vascular permeability leads to abnormal fluid collection within or below the retina that causes visual dysfunctions when it involves the center of the macula.

- *Glaucoma* is primarily a neuropathy not a retinopathy, and it is characterized by gradual damage to the optic nerve with consequent damaging of ganglion cells and their axons. From a visual analysis glaucoma manifests itself as a structural deterioration of the optic nerve head (ONH); the ratio of the optic disc cup and neuroretinal rim surface areas is an important structural indicator for assessing the presence and progression of glaucoma.

- *Cardiovascular diseases*, such as hypertension and atherosclerosis, might cause several changes on retinal vasculature structure: decrease of the ratio between the diameter of retinal arteries and veins, which increases stroke risk and myocardial infarction, retinal ischemia and arterial and venous occlusions.

- *Retinopathy of prematurity (ROP)*, is a disease which affects premature infants and is characterized by abnormal development of retinal vasculature, that eventually leads to retinal detachment and visual loss. Retinal structural features such as tortuosity and vessel width are widely studied in the literature to improve clinical diagnosis and evaluation of ROP.

CHAPTER 2: HUMAN SCHISTOSOMIASIS

2.1 SCHISTOSOMA AND SCHISTOSOMIASIS

Schistosomiasis is a tropical disease considered by the World Health Organization as the second most socioeconomically devastating parasitic disease, next only to malaria. It is caused by worms of the genus of tremadotes, the Schistosoma; adult schistosomes are greyish or white flat worms of 7-20 mm length with cylindrical body. Unlike other trematodes, schistosomes have separated sexes, the male's body forms a groove in which it holds the longer and thinner female; they feed on blood and globulins through anaerobic glycolysis and debris are regurgitate in the host's blood. Females deposit in the human body hundreds to thousands eggs per day, each ovum contains a ciliated *miracidium* larva which secrets protolithic enzymes that help the eggs to migrate into the lumen of the bladder or the intestine. The eggs exit the human body through the urine or the faeces and when in contact with the water they release the *miracidium*, which searches for the intermediate host, freshwater snails. After 4-6 weeks the miracidia leave the snails as *cericarial*, which spin around the water for up to 72 h seeking the skin of a suitable definitive host. An infected snail can release into the water thousands of cericarial a day per months. Once the cericarial penetrate the skin, it reaches the blood flow and transforms into young worms or schistosomulae and the cycle starts again.

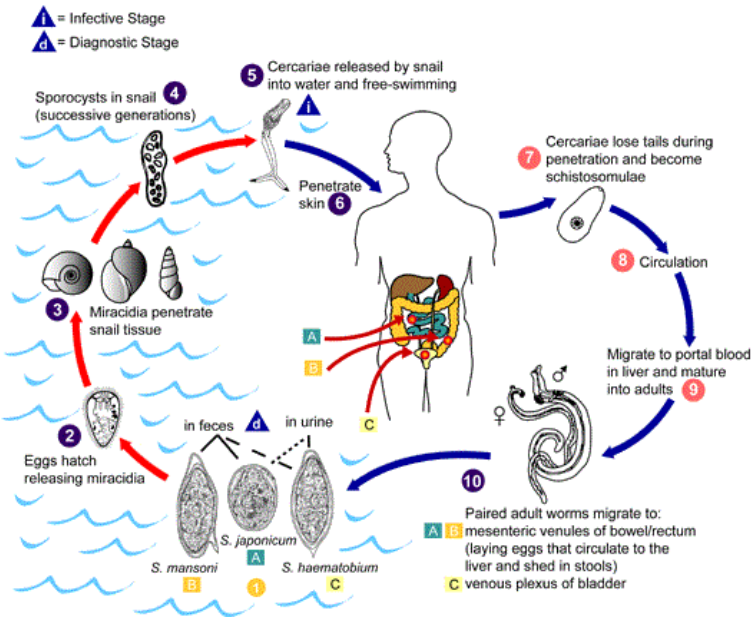

Figure 2.1: Schistosoma Life Cycle

The main schistosomes infecting human beings are: *S. mansoni*, which is transmitted by *Biomphalaria* snails and causes intestinal and hepatic schistosomiasis in Africa, South America and the Arabian Peninsula; *S. Haematobium*, transmitted by *Bulinus* snails and causing urinary schistosomiasis in Africa and the Arabic peninsula; and *S. japonicum*, transmitted by the amphibian snail *Oncomelania* and causing intestinal and hepatosplenic schistosomiasis in China, the Philippines and Indonesia. The disease is largely a rural problem, with higher infection rates in children than in adults.

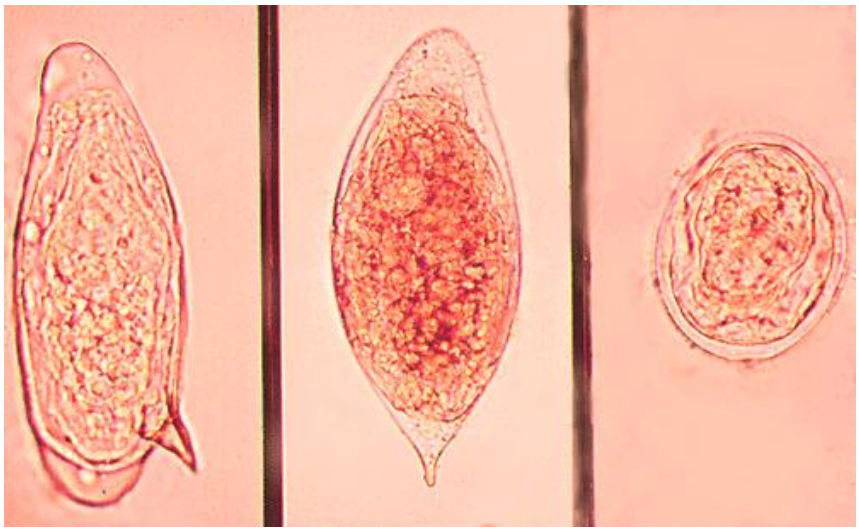

Figure 2.2: different kind of Schistosomes: from left to right S. mansoni, S. haermatobium, S. japonicum

The disease occurs in two phases: chronic or acute. The chronic phase affects mostly patients living in the endemic area while the acute phase usually occurs in individual who have recently visited the endemic area without having had any previous contact with the parasite. In the chronic phase most of the patients are asymptomatic only few develop the sever form of the disease. The acute phase occurs few weeks or months after a primary infection and starts with fever, myalgia and cough; while many patients recover spontaneously after few weeks, some patients can develop persistent and more serious symptoms such as weight loss, diarrhea and diffuse abdominal pain.

2.2 SCHISTOSOMIASIS MANSONI

Schistosoma mansoni is responsible for liver lesions that can alter the hemodynamic of the portal venous circulation, lung arterial and venous systemic system. A number of secondary phenomena occur with portal hypertension, the fundamental initiating factor is an increase resistance to portal venous flow. Therefore it has been suggested that ocular circulation may also suffer from hemodynamic alterations in schistosomotic patients causing ischemia of the retina, damage to the layers and tortuosity. The hemodynamic repercussions of portal hypertension have been discussed in some studies, which have shown delayed fluorescein uptake in the retina of patients with schistosomiasis, which suggests that arterial irrigation of retina is jeopardize by increased capillary blood pressure. In a case study, Delgado AC et al [1], tried to determinate the fluorescent contrast arrival time at the retina of young patients with the hepatosplenic form of schistosomiasis mansoni. Results were compared for a group of patients affected by the disease and a group of non-schistosomotic patients pared for age. In both groups were found relative retardation of contrast arrival time while only in the schistosomotic patient group were found few cases of absolute retardation. The results obtained, even though statistically not significant, probably due to the limited number of patients that undergo angiography aged between 10 and 21 years old, suggest delayed blood flow of retina.

CHAPTER 3: RETINAL IMAGE ANALYSIS

3.1 RETINAL IMAGE ANALYSIS TOOLS

The retina represents indeed the best example of body window, through which is possible to visually inspect, in an easy, fast, non-invasive way, the inner region of the human body, and in particular the micro-circulation and its possible alterations. Recent development in the field of medical images processing has allowed to identify and to analyze many features related to the retinal vascular system. Width, caliber, branching angles and tortuosity are some of the parameters which are used to characterize the vascular system itself and eventually to predict vascular diseases. These parameters are closely related one another and each of them carries basic information necessary to describe potential diseases and their development. Several tools and software have been proposed over the last few years that provide a semi-automatic quantification of these properties and other retinal landmarks such as the optic disc location and the vasculature network. One of the advantages these tools offer is the chance to process images in an objective and efficient manner, whereas tracing manually the images may slow down significantly the analysis.

From an international collaboration between the University of Dundee, Edinburgh and Palermo it has been developed the software VAMPIRE (Vessel Assessment and Measurement Platform for Images of the Retina) [3]. VAMPIRE is an easy-to-use tool whose interface provides easy-to-understand visual feedback of the features extracted and a set of tools that allows the user to easily identify, locate and correct wrong measurement; moreover no experience of image processing algorithms is assumed. The software at first operates in order to locate key retinal landmark, namely the optic disc and the approximate path of the arcade vessels. Then the location and representation of the vasculature network; several vessel detection algorithms have been tried and finally it was decided for an implementation which was a good compromise between speed and accuracy. VAMPIRE offers also an assessment to vessel width and tortuosity. The width is computed as the length of the cross-section of the vessel mask taken perpendicularly to the vessel's estimated axis while tortuosity measures integrate axis curvature and vessel width [11]. Along with these estimates other measures are available with the software, or are been developed in order to be incorporated.

The ultimate vision of the research group is to make VAMPIRE available as a public tool; the team is currently working in order to extend the validation of VAMPIRE modules, gathering increasingly extensive collections of images, catalogued by different attributes and annotated by multiple experts.

A research group of the University of Padua has proposed in the last few years more than one tool for detecting a certain number of retinal parameters, moreover their aim has been to developed them as a web-based tools. The team, headed by Alfredo Ruggeri, has proposed three tools: the ARVnet system, the TorTnet system and the ROPnet system [4]. The ARVnet system provides an estimate of the articular-venular ratio (ARV) which is an index for arteriolar narrowing, one of the first sings to appear in retinopathy from hypertension and diabetes. The ARVnet system offers a much shorter computational time if compared with other popular software.

The TorTnet system has been thought to measure first the tortuosity of a single vessel then, combining the estimates of all the vessels of the image, a value of tortuosity for the whole image. The ROPnet is a web-based system which provides assessment of vascular width and tortuosity in ROP images [5]; the user is able to select an image from its own folder, which is sent to the server and temporally stored until the analysis is finished. Through the tool the user select a vessel by quickly drawing a curve that approximates the position of its centerline and the software automatically extracts a region of interest (ROI) around the selected vessel, in order to limit the processing area and thus reduce the computational time. Finally the vessel centerline is extracted along with an assessment of the caliber and the tortuosity of the vessel selected.

For our case study we have decided not to use any of the available tools; in fact most of them provides a description of the vascular network where vessels are divided in segments. To assess a tortuosity measure based on the frequency content we needed vessels to be less fragmented as possible, in order to have an overall complete frequency description.

3.2 TORTUOSITY

We have decided to focus our attention on tortuosity which is a phenomenon that characterizes all the blood vessels on human body, from the tiny little vessels of the retina to main vessels, such as the cervical carotid arteries, the cerebral vasculature and other mayor arteries and veins. It has been proved that changes of tortuosity of retinal vessels might be signs of alteration or improvement of certain diseases such as retinopathy of prematurity (ROP), diabetic retinopathy or hypertension.

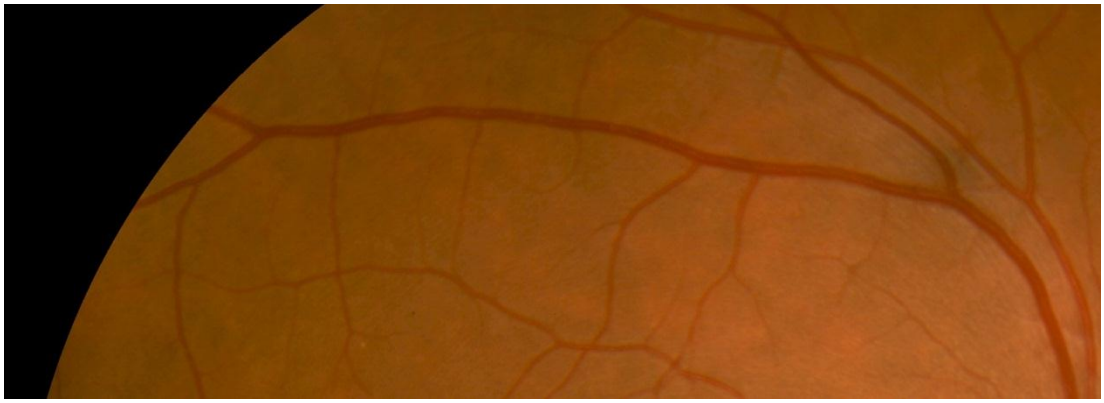

Figure 3.1: An Example of Non-tortuous Vessel

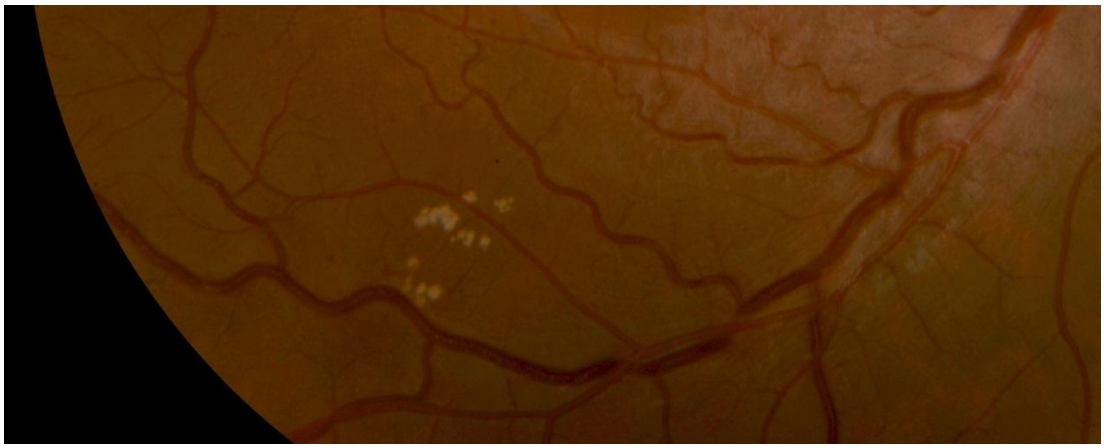

Figure 3.2: An Example of Tortuous Vessel

C.S. Cheung et al [6] in their case study have demonstrated how to tortuosity it is an index of the severity of ROP, especially in more severe cases such as those with plus disease. They computed two different measures of tortuosity: central (within 2 disk diameters from the center of the optic disc) and paracentral (form 2 to 4 disk diameters), and they proved that, especially arteriolar tortuosities in both central and

paracentral regions, were more sever in patients with more advanced form of ROP. They also compared tortuosity values before and after a laser treatment, dividing vascular variables between pre-plus and plus disease; comparing arteriolar tortuosity they found a significant difference between both groups and regions of the retina, whereas in case of venular tortuosity a significant difference has been found only in the paracentral region.

M.T. Cabrera et al [7] compared five different methods to establish the best way of combining retinal vascular tortuosity and width measure in order to quantify an qualify plus disease. In another case study C.Y. Cheung et al [8] tried to describe vascular tortuosity estimate and their relation with age, blood pressure and other cardio vascular diseases in a sample of population aged 40 to 80 years. They used a computer assisted program (SIVA version1.0) to obtain several retinal parameters in a region from 0.5 to 2.0 disc diameters around the optic disc. As result they extracted a correlation which shows the trend of tortuosity to decrease with the age, both in the arteries and the veins, while on the other hand tortuosity decreases with mean arterial blood pressure in the arteries and increases with the veins.

M.B. Sasongko et al [9] conducted a study on 327 patients aged 18 to 70 years, 224 with diabetes and 103 without. Part of the participants affected by the disease was also affected by diabetic retinopathy (DR). The aim of the study was to establish how tortuosity is related with diabetes and DR, which has been categorized into mild non-proliferative DR (NPDR), moderate DR and vision threatening DR (VTDR). It has been observed that patients affected by diabetes manifest more tortuous retinal vasculature than healthy one; and in those with diabetes a higher level of arteriolar tortuosity has been detected in case of mild and moderate stages of DR.

3.3 Measure of Tortuosity: Related Works

Clinicians use tortuosity as a parameter to define how winding and twisted vessels - are, classifying vessels on a four to five level scale of tortuosity. However as a subjective estimate tortuosity is not quantitative defined in the medical literature thus many models and possible tortuosity measures have been proposed in order to describe clinicians' intuitive observations. All these methods are based on manual or

semi-automatic techniques of tracing blood vessels and almost all of them compute a local measure of tortuosity eventually improving the assessment relating tortuosity with other vessels caliber or width.

L. Hathout et al [10] of Stanford University observed general uniformity of vessels shapes and curvatures across multiple vessels and different individuals. They hypothesized the idea of some principles which govern the shapes of the vessels and they research a mathematical model to describe their behavior. The implemented a model which was originally developed in the field of geophysics to analyze the mending of rivers. They extracted curve specific parameters, such as path length, wavelength and radius of curvature, which are combined and used to test the model against normal vessels segment. Eventually the model is applied on a known case of abnormal vascular tortuosity to verify its reliability in identifying and quantifying deviation from normal cases. The curve they found it's known in mathematics as "sine-generated" curve, it is not a sine or cosine curve, it rather belongs to a class of functions which describe a curve by specifying its "direction" angle. And they proved that if the sine-generated curve is a good approximation of the selected vessel profile, there is a close correspondence between theoretical values and those measured for the vessels.

E. Trucco et al [11], in their research work suggested that vessels caliber play a relevant role in defining the tortuosity along with the curvature. They observed that vessel thickness affects the maximum allowable curvature of the vessels and also that thicker vessels are characterized by thicker wall, so it is required a higher effort to bend a thicker vessel than a thinner one. The method proposed consists in two steps, at first the location and characterization of the target vessel and secondly the estimation of vessel tortuosity. Hence vessels boundaries are detected, starting from the vessels skeletons and the curvature, by interpolation with cubic B-splines. They firstly computed tortuosity without considering the caliber, in order to compare the outcomes with previously related work, then a final estimate combining both curvature and thickness. The results obtained revealed a good correspondence with clinical judgments proving that other factors, rather than curvature, may be considered for tortuosity measures.

A. Bhuiyan et al [12] proposed another method for tortuosity assessment based on vessels width, as E. Trucco and his team [11]; they noticed that tortuosity is more marked in narrower vessels than in wider ones so they suggested a tortuosity measure computed on vessel-segments edge, proving how width can affect vessels bending capability. Hence starting from the vessel centerline, for each point they detected the width and the pair of pixels belonging to the edge. Once the vessel edges are defined, for each pair of pixels they measure the absolute angle difference in order to obtain the average angle which is the tortuosity for the selected vessel-segment.

A further step on the tortuosity field has been done by W.E. Hart et al [13]; they tried to achieve a tortuosity estimate for both single vessels and vessel network. Their working method is based on three properties that describe ophthalmologist intuitive observation:

- *invariance to translation and rotation*, which assumes that vessel tortuosity does not depend on the location orientation of the vessel;
- *response to scaling*, which assumes that vessel tortuosity should be invariant to scaling, and if scales does affect the measure then it does so in a multiplicative manner;
- *vessel compositionality*, which assumes that a vessel composed of two segments with different tortuosity, should be characterized by a degree of tortuosity between the tortuosity of its constituent segments.

Eventually they computed and compared a set of tortuosity measures, based on general curves descriptors, in order to define the relevance of the proprieties. These techniques have been used for segments, single vessels and vessel networks tortuosity; on their experimental results the authors demonstrated how proposed measures can be used with effectiveness for tortuosity based classification.

A different approach to the tortuosity assessment has been presented by Martin Rodriguez et al [14], they introduce the spectral analysis as a means to evaluate the winding degree of the aorta from a 3D image. Their method describes tortuosity as the fast Fourier transform (FFT) of the local curvature of the vessel path. For each point of the vessel centerline they calculated the local curvature as the ration between the acute angle defined by the tangent vectors of two consecutive points and their

Euclidean distance. The overall curvature was calculated as the sum of curvatures at each constituent point of the centerline; hence the global value of tortuosity for a vessel has been calculated as the spectral analysis of the global curvature. The Idea was that a straight vessel would have a null coefficient of tortuosity and a flat amplitude spectrum implying absence of tortuosity, whereas a sinusoidal vessel would have an amplitude spectrum with a single peak of fixed amplitude, corresponding to the main frequency. They tested the method both on phantom centerline and clinical data revealing a good correspondence and effectiveness of the method.

CHAPTER 4: DATA SET DESCRIPTION

4.1 IMAGE CLASSIFICATION

The data set provided consists in about 300 images, recorded at clinic of Hospital das Clínicas da Universidade Federal de Pernambuco, from patients with different grads and kind of retinopathies. Three ophthalmologists (observers A,B,C) have been ask to classify the images of the data set according their own experience, and divide them in three classes : low-tortuosity class, normal class and high-tortuosity class. Excluding two images (1394, 4432), which have been classified only by the observe C and other two (1323 and 2166) which have been identified as belonging to different classes by all three observes, images have been classified as show in **Table 4.1**:

Class	Number of images
low	104
normal	154
high	44

Table 4.1: Number of Images per Class

An image has been classified as belonging to a certain class if at least two of the three observers agreed.

Obervers classification	Numer of images	%
all same	201	66,10
two same	101	33,20
all different	2	2

Table 4.2: Percentages of Agreement

As shown on the **Table 4.2**, on classifying 304 images the three observers agreed in the 66% of the cases, two out of three agreed on the 33% of the cases and only on the 2% of the cases the classification results were totally different (See appendix A for classification details).

4.2 IMAGE SELECTION CRITERION

In order to provide a clear characterization of each image and to compute reliable tortuosity estimate, it has been necessary to narrow the number of images provided for each class according to a well-established criterion, without losing any statistical significance. An early selection has been decided based on the quality of the images: to guarantee a clear detection of the retinal blood vasculature and a precise tracing of the vessels map, it was decided to discard out-of-focus images in which the distinction within artery or vein branches would be unclear to an observer. On the other hand it was decided to keep images with comparable fields of view, to provide a consistent comparison on the global tortuosity measures. Secondly the attention was focused on the temporal area of the retina. The selection proceeds according to the information in each image. Therefore we selected the images with at least two arteries and two veins of first level, each one has to be longer than twice the optic disc diameter and there has to be one artery and one vein on the superior half of the temporal area, and one artery and one vein on the inferior half. No restrictions are imposed on the number of vessel of second level considered.

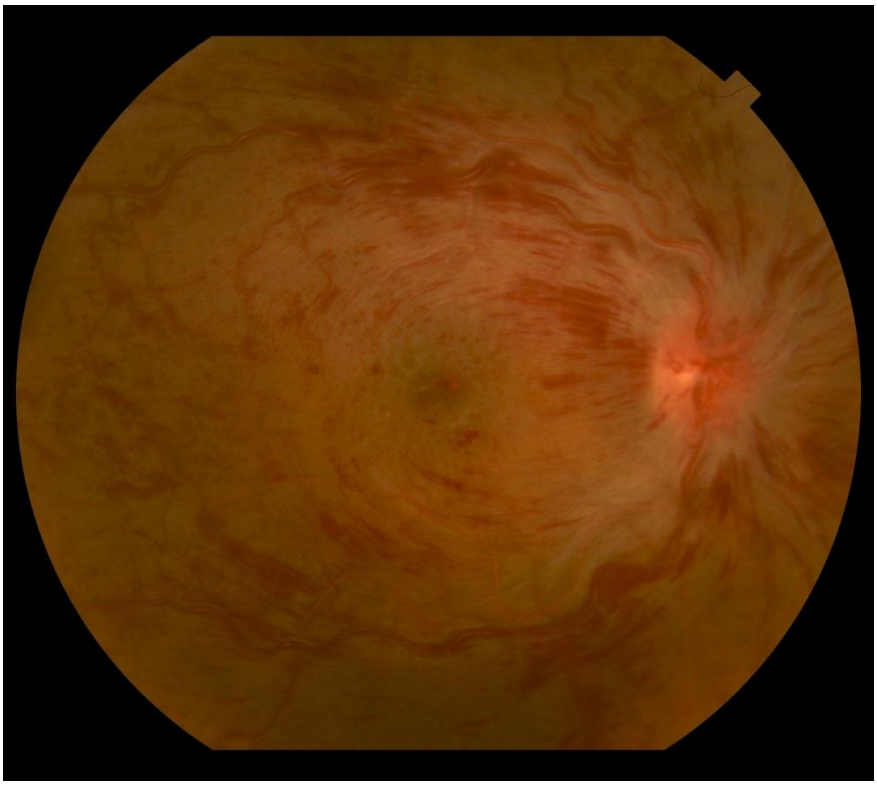

Figure 4.1: Example of discarded Image (image 1)

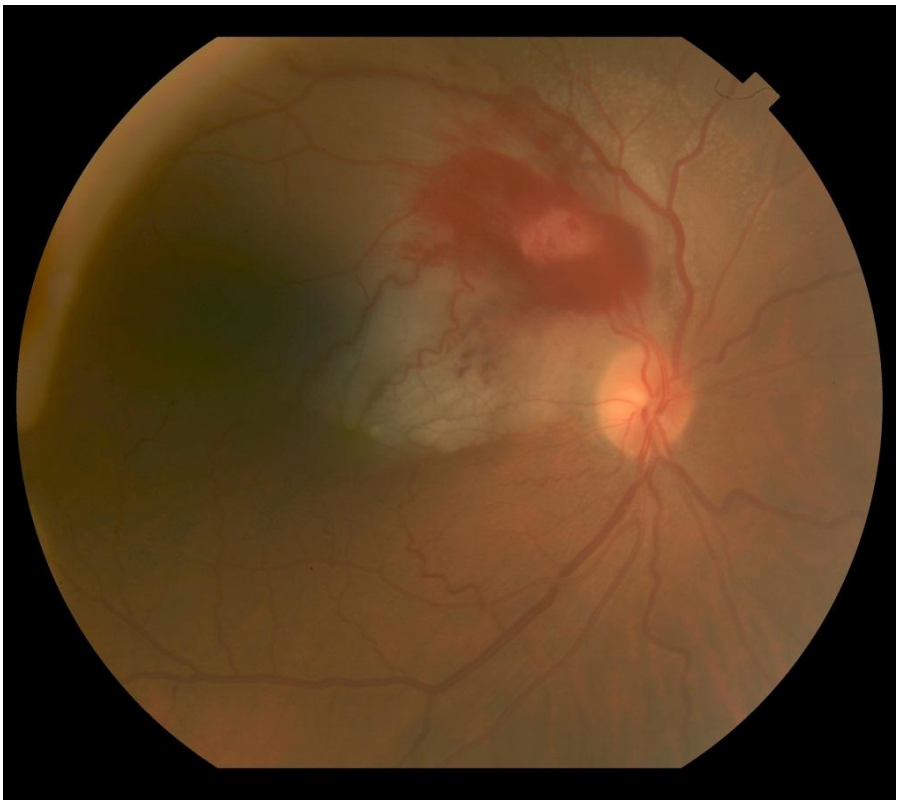

Figure 4.2: Example of discarded Image (image 404)

Figure4.3: Example of discarded Image (image 5644)

Following this procedure the classes have been reduced to fewer elements: 42 images in the low-tortuosity class, 34 images in the normal class and 24 images in the high-tortuosity class.

Observe classification	Number of images	%
all the same	20	47,62
two the same	22	52,38
Total images	42	

Table 4.3: Low Class Percentages of Agreement

Observe classification	Number of images	%
all the same	17	70,83
two the same	7	29,17
Total images	24	

Table 4.4: High Class Percentages of Agreement

Observe classification	Number of images	%
all the same	31	91,18%
two the same	3	8,82%
Total images	34	

Table 4.5: Normal Class Percentages of Agreement

These tables above show per each class how many images have been selected to be processed and the percentage of agreement among the observer in classifying these images.

Figure 4.4: Example of Low-tortuous Image

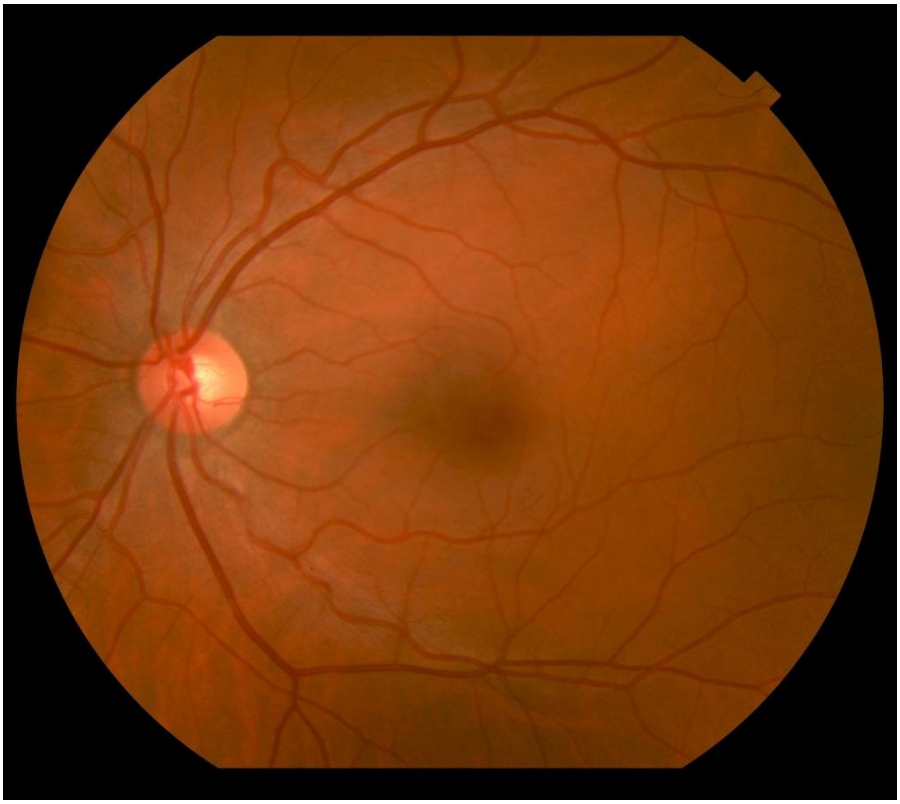

Figure 4.5: Example of Low-tortuous Image

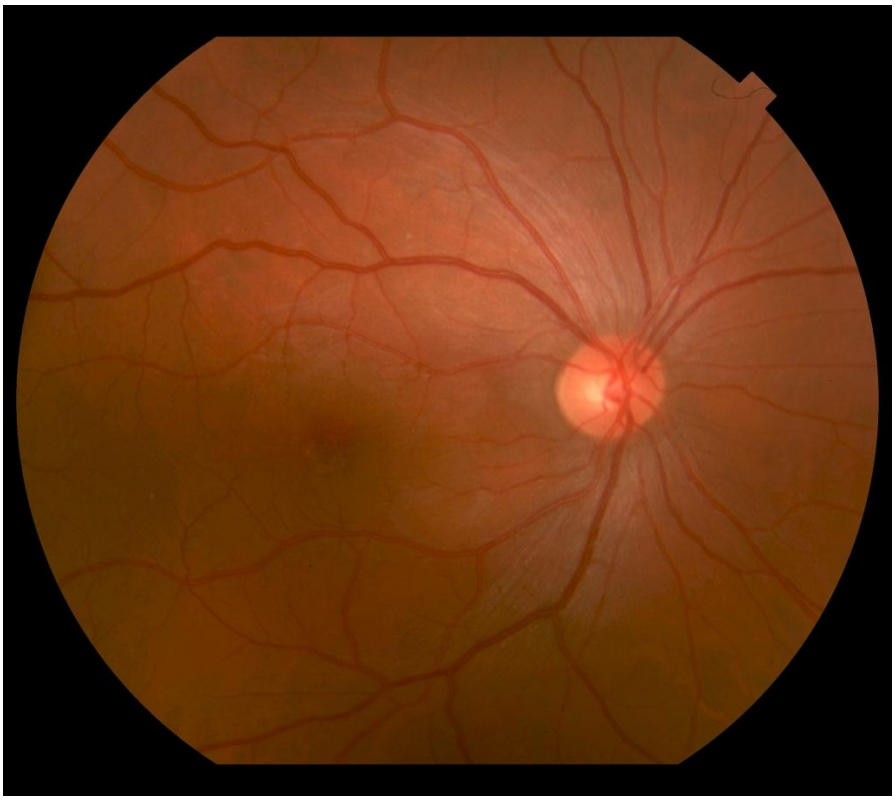

Figure 4.6: Example of Normal-tortuous Image

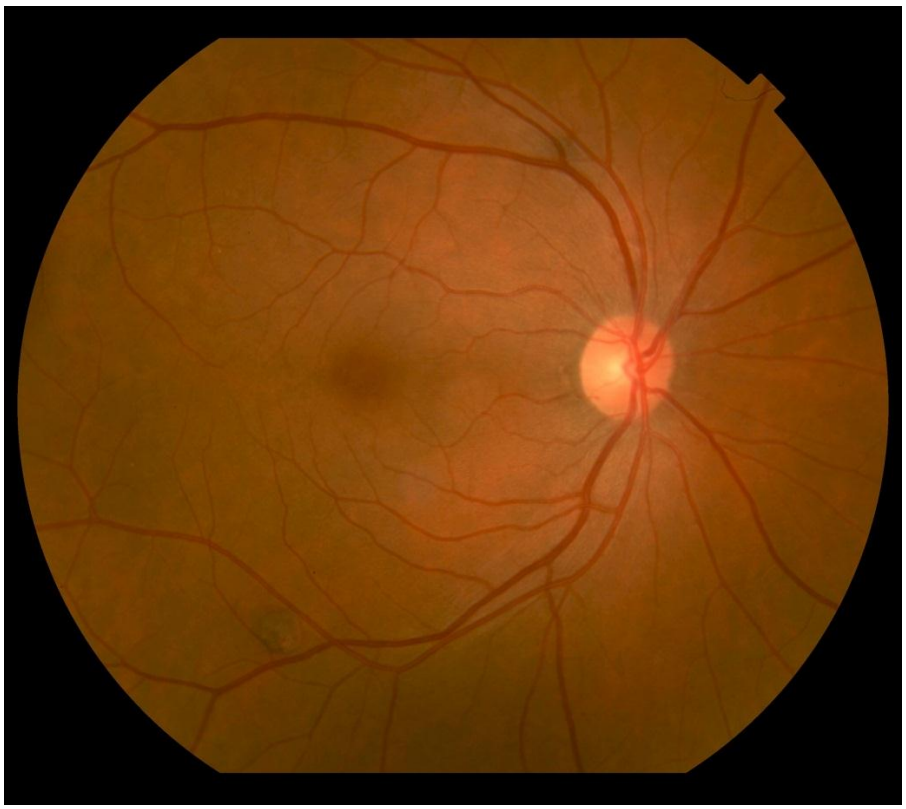

Figure 4.7: Example of Normal-tortuous Image

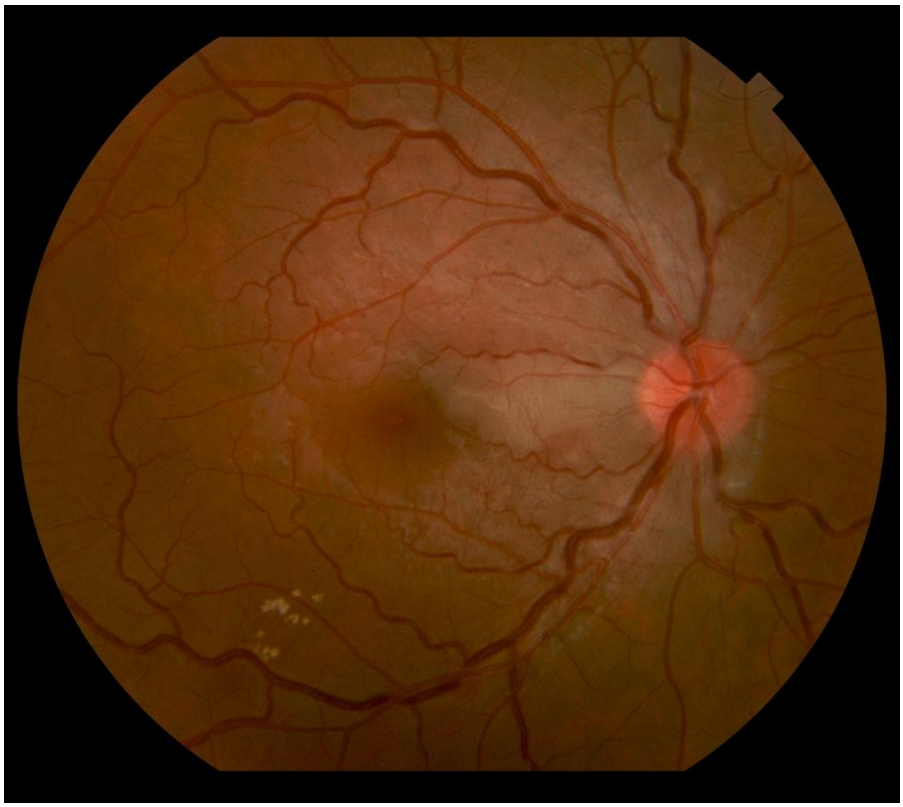

Figure 4.8: Example of High-tortuous Image

Figure 4.9: Example of High-tortuous Image

4.3 TRACING PROTOCOL

Once the selection procedure is over, each image is processed and the vessels tree is traced manually following a precise protocol. Starting from the proximity of the optic disc, first level arteries and veins are detected and traced until the junction is reached. At each branching point the main vessel proceeds along the wider path, whereas second level vessels spread through the retina and these are considered only if their length is at least equal to an optic disc diameter.One of the most significant differences between the manual and automatic selection of the vessels structure, is that by tracing manually it is possible to obtain a better defined and more reliable map and with longer segments. Moreover in order to obtain an accurate distinction between arteries and veins, it has been decided to trace arteries and veins in different colors (white for arteries and black for veins) and also to trace vessels into different image layers.

Per each images four different layers have been considered:

- 1^{st} and 2^{nd} layers contain main arteries and veins, hence those vessels whose paths starts from the optic disc and often reach the end of the field of view;
- 3^{rd} and 4^{th} layers contain secondary arterioles and venules, which are the smaller vessels whose path starts from the branching points of the principal vessels.

Analyzing four separate layers allows one to avoid overlapping segments and to process longer paths, which is significant for the analysis of the spectral components.

Figure 4.10: Example of Image with the Entire Network Traced, Arteries White and Veins Black

Figure 4.11: images 1 to 4 show separately the four different layer of the image showed in **Figure 4.4**; image 1) 1^{st} level arteries, image 2) 2^{nd} level arteries,

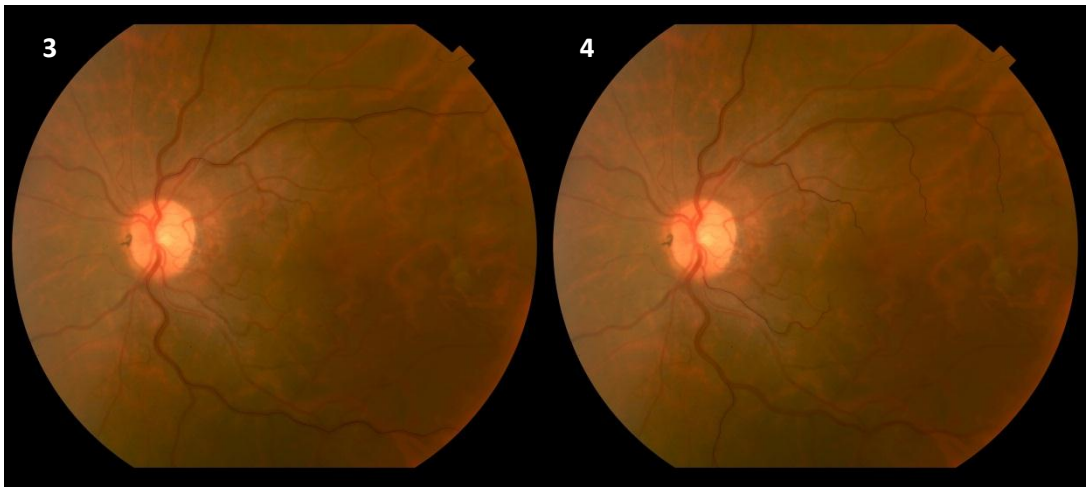

Figure 4.11: image 3) 1st level veins, image 4) 2nd level veins.

IMAGE ACQUISITION METHODS

Digital color fundus photographs (angle of coverage of 50°, 1024x1024 pixels) centered on the fovea, were obtained after pupil dilation with 1% tropicamide and phenylephine hydrocholoride 10%, using a model TRC-50DX fundus camera (Topcon, Tokyo) equipped with a digital back piece (CCD camera ; Allied Vision Technologies, Statroda, Germany) and a PC-based image-management system (IMAGEnet 2000™ Digital Imaging System, Topcon, Tokyo).

CHAPTER 5: ANALYSIS METHODS

5.1 INTRODUCTION

Once the images to process have been selected and the vessels traced, the image analysis starts. It has been decided to divide our work in three sections:

1. extraction of the vessels skeletons contained in each layer of the image;
2. processing of vessels skeletons;
3. Spectral analysis (FFT computation).

The three steps are strictly connected one another, the outputs of the first step are the inputs of the second one as well as the outputs of the second one are the inputs for the third. Nevertheless the choice of dividing them is due to practical considerations: firstly an easier understanding of the developed algorithm, secondly the thought of easier implementations or modifications of each part if needed.

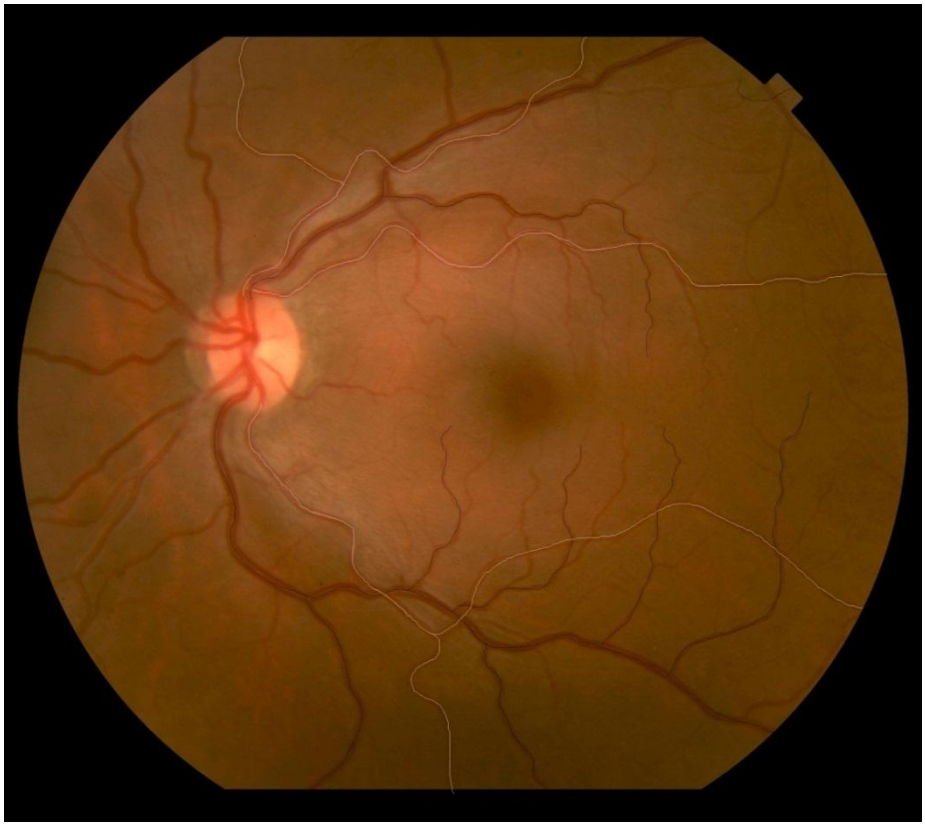

Figure 5.1: RBG Image

5.2 VESSEL SKELETONS EXTRACTION

It has been decided to work with the green level of the RGB image, since it has been notice to be the level which supplies a better definition of the vasculature network.

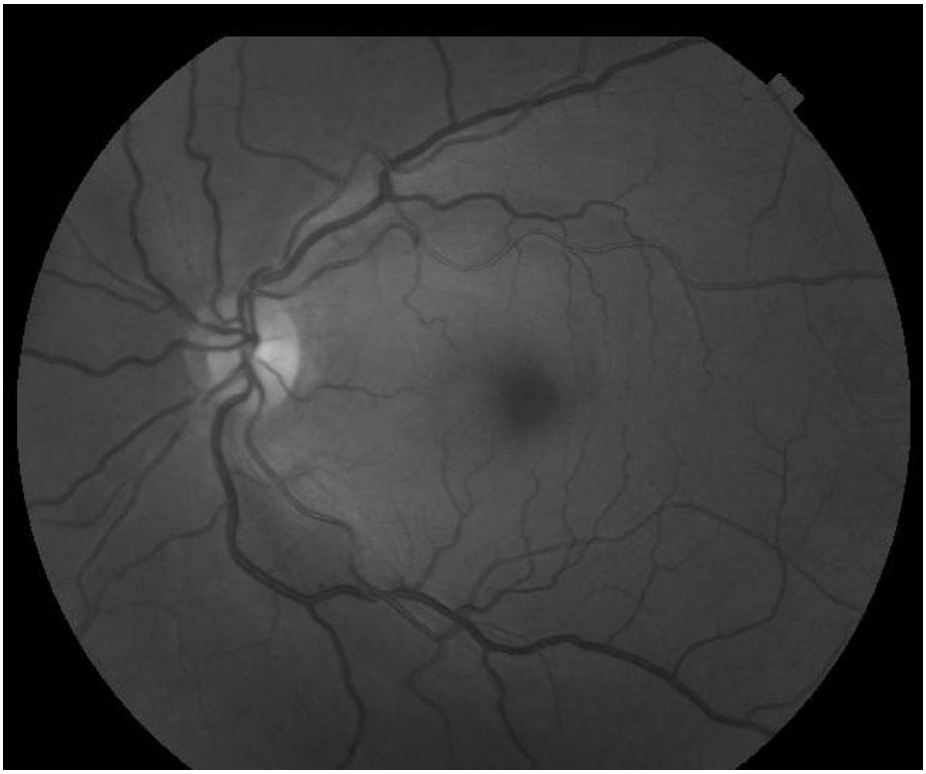

Figure 5.2: Green Level RGB Image

This section consists of four sub steps one for each of the four layers of the image. For detecting arteries and arterioles the image is converted in a binary mask (searching for the pixels with values equal to 255) where the vessels pixels are white (binary 1) and the background is black (binary 0).

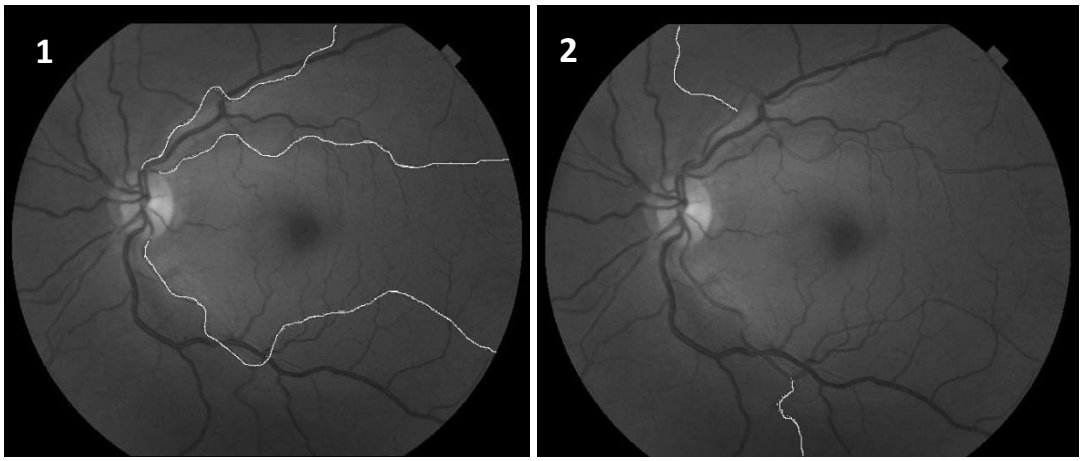

Figure 5.3: Image 1 and 2 show the 1st and 2nd level arteries that have been selected in the image

Moreover, on the binary image, it has been notice that white pixels appeared in the area of the optic disc and not only as belonging to the vessels skeletons. Hence morphological operations are computed on the binary image in order to remove all the connected components that belong to the background and are not part of the arterial network.

At this point the Matlab function *bwareaopen* has been used and a threshold of 100 pixels has been set, so all the connected components with less the 100 pixels have been removed. Eventually the remaining connected components are the skeleton of the vessels network; these have been labeled and counted in order to assess how many arteries and arterioles there are in the current image. The following two steps are dedicated to the extraction of veins and venules, these are slightly different from the previous ones since veins and venules have been traced in black on the original RGB image.

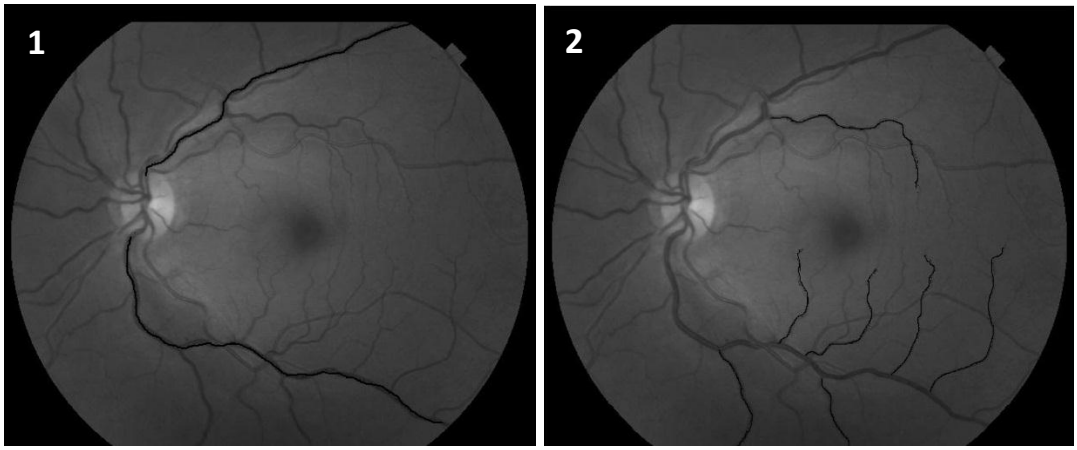

Figure 5.4: Image 1 and 2 show the 1st and 2nd level veins that have been selected in the image

As done previously we extract a binary image which is processed in order to remove all the pixels and connected components that belong to the background, by mean of the function *bwareaopen* and using the same pixels threshold.

While extracting the binary image for veins and venules, considering that veins are traced in black we search for pixel value equal to 0; this leads us to a binary mask where the background is black, as desired, while the vessels and the border are white. In order to extract form the binary image only the white pixels belonging to the vasculature network it has been computed a compensation of the border.

So it has been extracted a complementary binary image with a black border (binary 0) and a white background (binary 1). Then the first binary image has been multiplied with the second one, and the result is a binary image with white vessels on a black background, which includes also the border. Finally the vessels skeletons are labeled and counted in order to assess how many veins and venules there are in the image.

This analysis has been computed for all the images of the data set and the outcomes are saved in a structure, one per each image, which contains a set of information regarding the image:

- The name of the image as *"number-tortuosityClass"*;
- The number of vessels globally detected in the image;
- Information about each single vessel: pixels of the centerline, the kind of vessels (A/V) and whether it is a main vessel (1^{st} level vessel) or a secondary vessel (2^{nd} level vessel) and a label which counts the vessels detected in the image.

These structures and the information contained have been used as inputs for the following step of the analysis.

5.3 VESSEL SKELETONS ELABORATION

To ensure a consistent Fourier Transform for all vessels, some work has been done on the vessels centerlines which have been detected form the RGB image. It has been noticed that each vessels are characterized by a well-pronounced elongation direction, along which they can be regarded as graphs 1-to-1 functions.

Hence it has been decided to transform the vessel centerline points into their PCA reference frame. Then we resample to guarantee uniform spacing and to eliminate points, if any, where one abscissa corresponds to two ordinate, obtaining a final series of samples x= 1...N and y = x(1)...x(N).

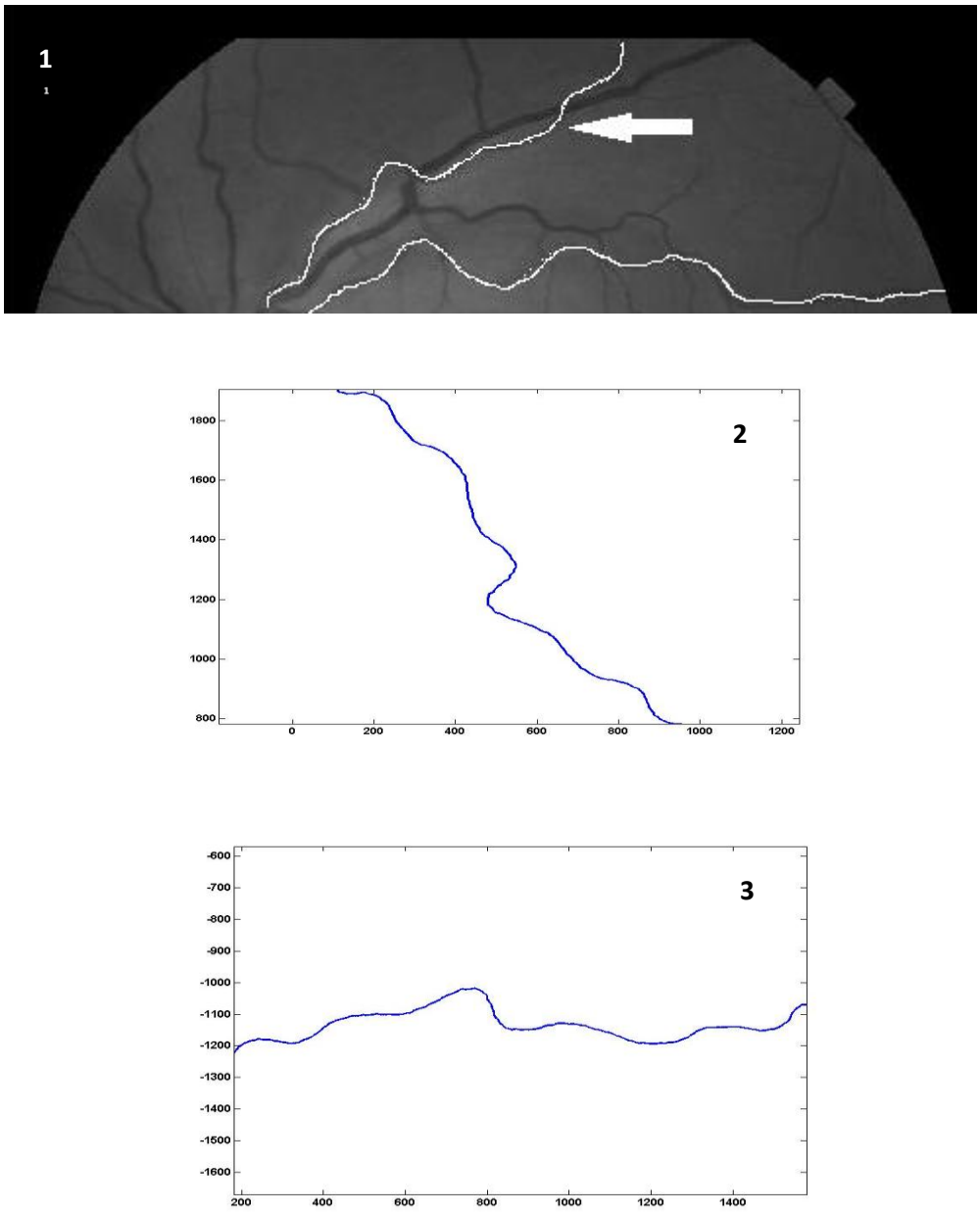

Figure 5.5: Vessel selection and PCA rotation

It has occurred in some cases that after the PCA vessels skeletons are not yet a 1-to-1 function, some abscissas correspond to two or more ordinates. So it has been decided to part the vessel at the point where the problem occurs. In order to identify the exact point of the skeleton it has been computed the difference of consecutive pixels of the skeleton itself, and the division was done when the difference was greater than 20 pixels. At first the vessel is divided in two parts, and each segment of centerline is transformed in its PCA reference frame. At this point each segment is subject to two controls: at first the length of the segment is checked and secondly it has to be verified that the segment is finally a 1-to-1 function.

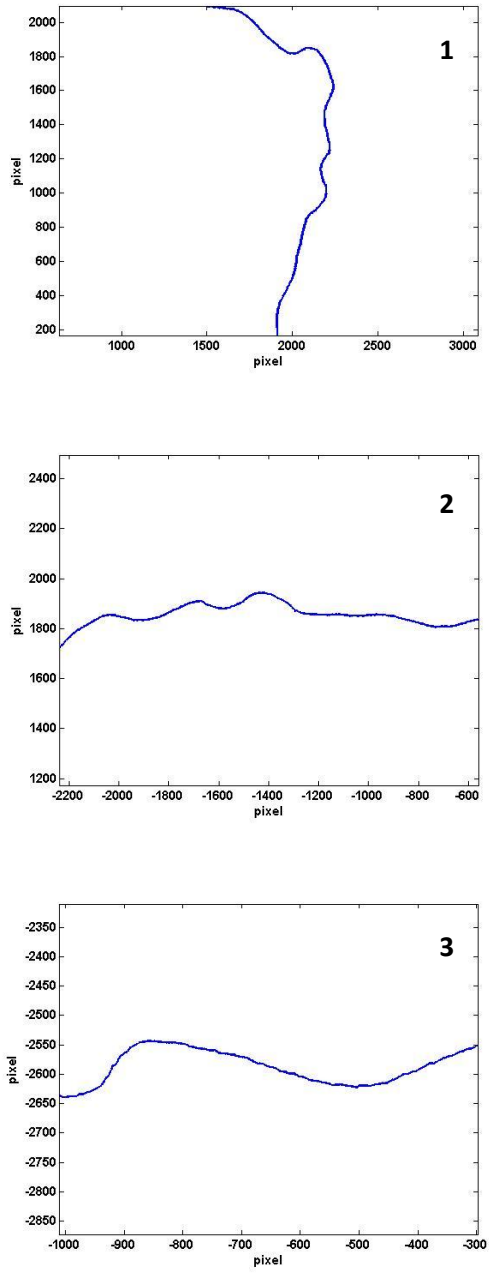

Figure 5.6: Vessel splitting after PCA

After a qualitative control it has been recognize a maximum significant frequency, for retinal vessels, of *1/100 [1/pixels]*; hence any higher frequency must be recognize as noise, mostly due to the manual tracing of the vessels map. This observation has leaded us to the decision to discard all the segments shorter than 100 pixels, because obviously they do not bring a significant contribution in terms of frequency. The segments which have not been discarded are now checked to be 1-to-1 functions; if so they are saved as part of the vasculature network of the image otherwise they are

divided again. The sub-segments obtained at this second division have been observed to be 1-to-1 functions so it has been done only a selection according to their lengths before proceeding with the resampling. The outcome of this section is a structure which contains information about the image vessels but this time each image will be generally characterize by a number of vessels greater than previously.

5.4 Spectral Analysis

So far in literature methods have been proposed for measuring the tortuosity of segments of vessels; we are now trying to compute at first the tortuosity of an entire vessel, secondly to assess the tortuosity of the full vascular network. This third and final section of our study is dedicated to the spectral analysis; Fast Fourier Transform (FFT) is computed on the skeletons of the vessels detected through the first two steps.

Once the FFT is computed on a vessel, the absolute values of the Fourier transform coefficients capture the frequency content of a signal, in this case vessel skeletons, providing a complete description of its frequency of change. For assessing the tortuosity of the whole image we thought reasonable to sum the absolute coefficients of the FFT of all vessels in order to have a global frequency description. To compute the sum of the Fourier coefficients it has been necessary to resample the spectra and interpolate it on a well-defined range of frequency. As mentioned before, it has been detected, form a qualitative analysis, a maximum significant frequency of *1/100 [1/pixels]*, and this value has been used to select only the most significant part of the spectrum. It has been decided to cut the absolute values of the Fourier transform at a range of frequency equal to the double of the maximum frequency, considering noise any other frequency component.

CHAPTER 6: FINAL RESULTS

6.1 INTRODUCTION

Schisostoma mansoni has been proved to be responsible for lesion that can alter the hemodynamic of the portal venous circulation, lung arterial and venous systemic system. Therefore, hemodynamic changes in the ocular circulation of mansonic schistosomotic patients with portal hypertension and hepatofugal venous flow are also probable. The aim of this research project is to propose a measure of tortuosity of an entire retinal image in order to be able to compare the semi-automatic analytic results with the results of the classification done by ophthalmologists. The method we adopted for assessing tortuosity is based on the spectral analysis: frequency content of vessels has been investigated as an index of how much winding and bending vessels centerlines are. Once the tortuosity of all the vessels traced within the image has been calculated, a global measure of tortuosity for the whole image has been proposed: the coefficients of the absolute values of the spectra of all the vessels have been summed obtaining an overall spectrum.

6.2 TORTUOSITY OF INDIVIDUAL VESSELS

In this first section we are going to discuss and evaluate the effectiveness of the spectral analysis as a technique to describe the tortuosity of vessels, which have been investigated regardless whether they belong to a low-tortuous, normal or high-tortuous image. Most of the methods proposed in the literature describe tortuosity as single value, so it is possible to identify thresholds that allow classifying the vessel, according to its tortuosity degree, as highly tortuous, non-tortuous or low tortuous.

In our case each vessel is characterized by a spectrum which contains all the dominant frequencies, hence we are trying to classify not a single value but set of coefficients, which are the absolute value of the Fourier coefficients. What is reasonably expected is to find spectra of tortuous vessel to present greater picks in correspondence to higher frequencies, whereas vessel with lower degree of bending will be characterized by higher picks only in correspondence of lower frequencies.

In order to verify our expectation the spectra of different vessels have been compared:

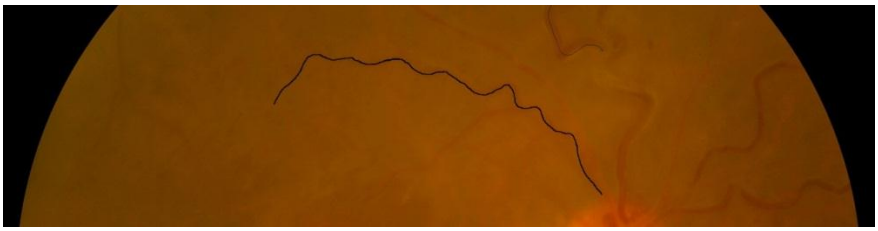

Figure 6.1: Tortuous Vessel

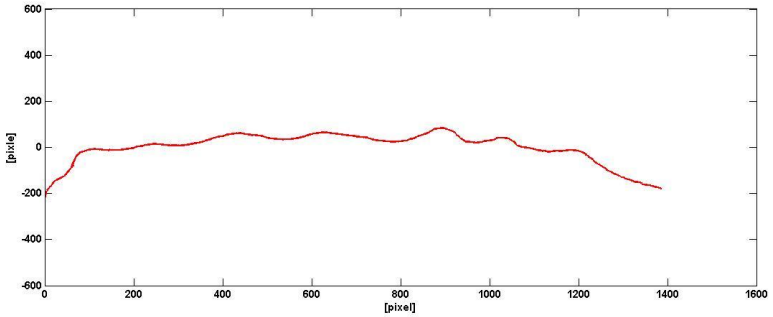

Figure 6.2: Skeleton of the Vessel in Figure 6.1

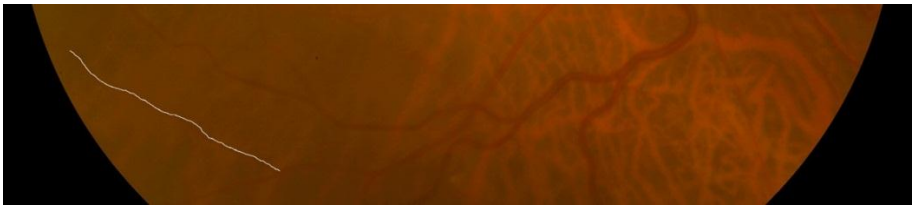

Figure 6.3: Non-tortuous Vessel

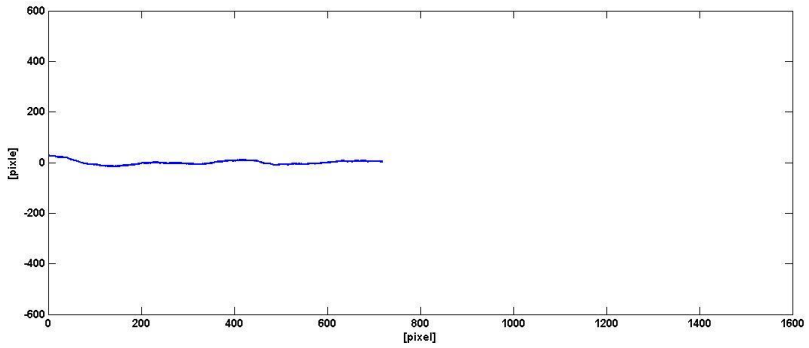

Figure 6.4: Skeleton of the Vessel in Figure 6.3

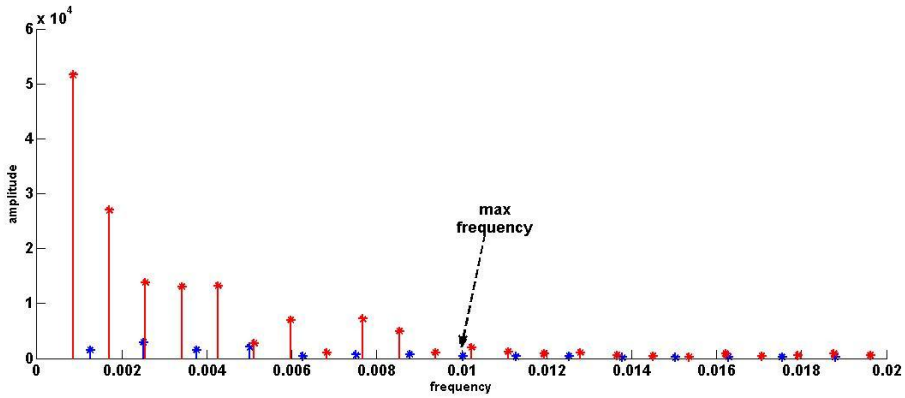

Figure 6.5: Compared Spectra of the vessel in Figure 6.1-2 and Figure 6.3-4

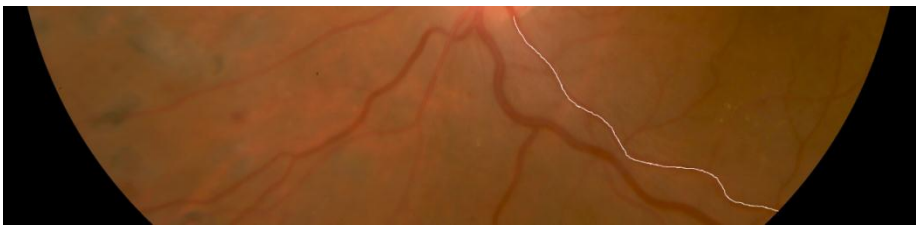

Figure 6.6: Long and Medium tortuous vessel

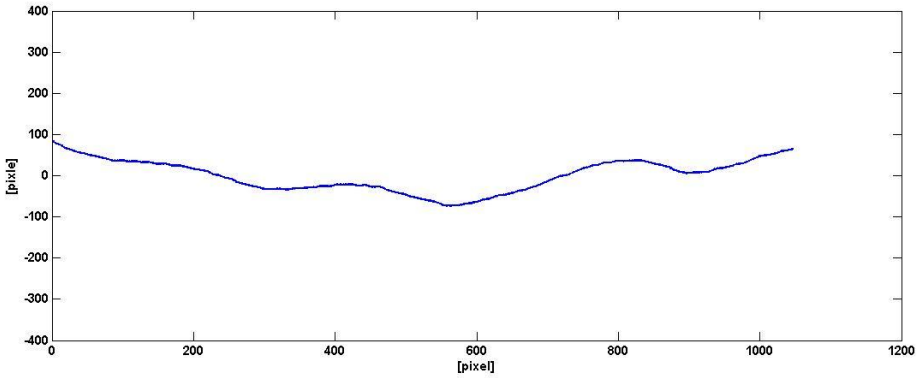

Figure 6.7: Skeleton of the vessel in Figure 6.6

Figure 6.7: Short and Medium-tortuous Vessel

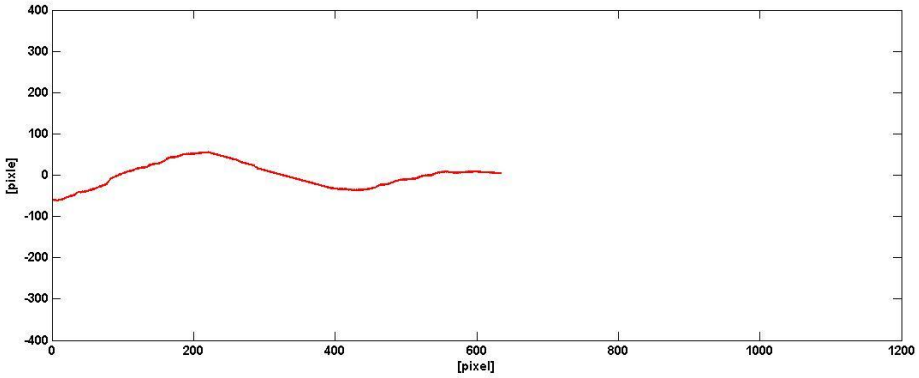

Figure 6.9: Extracted Skeleton of the Vessel in Figure 6.7

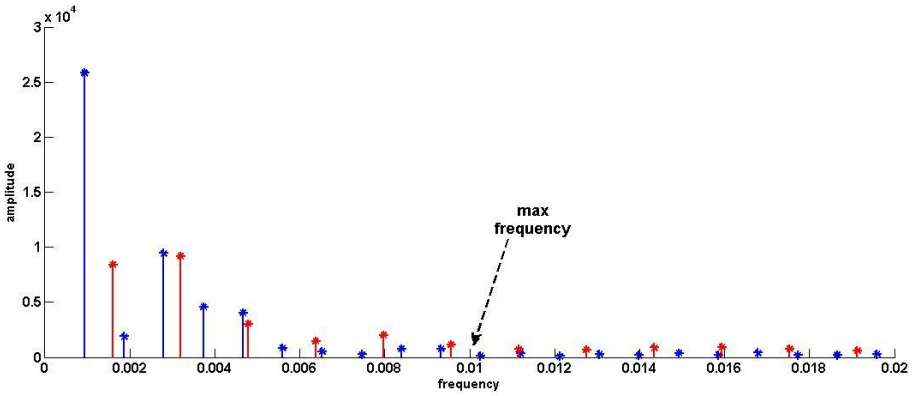

Figure 6.10: Compared Spectra of the vessel in Figure 6.6-7 and Figure 6.8-9

On Figure 6.5 and Figure 6.10 the spectra of four different vessels have been compared; Figure 6.5 shows the spectra of two vessels with different length and different degree of tortuosity, while Figure 6.10 shows the spectra of two vessels of different length but a similar degree of tortuosity. In Figure 6.5 it can be noticed a great different between the two spectra: the red spectrum, which belongs to the longest and more tortuous vessel, is characterized by higher pick even at higher frequencies. On the other hand the blue spectrum, which belongs to a shorter and less tortuous vessel (nearly a straight line), is characterized by lower picks.

On Figure 6.10, where vessels have similar degree of tortuosity, even the spectra are much more alike. Moreover in both Figure 6.5 and Figure 6.10 it can be noticed that the most significant frequency contents are located at frequencies lower than *f=0.01*; this fact confirms our qualitative observation according to which frequencies higher than 0.01 have to be considered as noise.

6.3 TORTUOSITY OF THE FULL VASCULAR NETWORK

Once they have been proved to be reliable in distinguish the frequency content of vessel centerlines, the spectra have been combine in order to obtain a frequency description for the entire image. Thus each image of the data set is described by a set of 100 coefficients, which are the absolute values of Fourier coefficients and are used as features to describe the tortuosity of the whole image and for classification tests.

A first attempt of classification has been done using the SVM classifier and the classification done by medical experts, who annotated and divided the images in the three classes, low, normal and high. Two approaches were used to select the optima subset of coefficients for classification:

- *Increasing by 20*: 5 tests were carried out, where the number of coefficients was increased by 20 (20,40,60,80,100) for every test;
- *Sliding by 30*: 8 test were run to test a subset of 30 coefficients which slide along the range of 1-100 coefficients (1-30, 11-40, 21-50, 31-60, 41-70, 51-80, 61-90, 71-100).

The best results achieved from SVM testing were from the *sliding 30* test in the range 1-30, with a confusion matrix

		predicted classes		
		normal	low	high
actual classes	normal	61.7647	32.3529	5.8824
	low	23.2558	48.8372	27.9070
	high	4.0000	28.0000	68.0000

Table 6.1: Confusion Matrix for the SVM classifier test

The results from the SVM testing have proved that the current approach needed to be reconsidered, so it has been decided to test a Naïve Bayer classifier with the aim of achieving better results with a simpler classification approach. The first attempt was a similar approach to the SVM search for best configuration of the coefficients; due to the simplicity and the speed of this classifier it has been possible to test 1115 combination of coefficients subset (with varied length and ranges, similar to what has been done for the SVM classifier). The confusion matrix shown below concludes that, while the Naïve Bayer method did achieve a gain in accuracy, the results are still too low for medical application.

		predicted classes		
		normal	low	high
actual classes	normal	79.4118	14.7059	5.8824
	low	37.2093	55.8140	6.9767
	high	12.0000	32.0000	56.0000

Table 6.2: Confusion Matrix for the Naïve Bayes classifier test

The failure of the two classification test has led to the conclusion that the poor results could be due to unclear or ambiguous annotations on the expert classification. So far the classification tests have been run considering the frequency content of all the vessels within the image, but the poor results have made us reconsider this thought and a second opinion has been asked regarding the classification done by ophthalmologists. With a more detailed classification it has been noticed that in some cases the early classification done by the ophthalmologists was uncertain (global agreement only on the 66%). It has been observed that sometimes, for classifying an image, the arterial component was more relevant than venous one (or vice versa). Therefore the expert classification has been enriched with a new set of annotation and new classification tests have been run.

The new approach split the data into 16 subsets according to the novel annotation: the images has been labeled as “certain” if all the ophthalmologists agreed on the classification, “uncertain” if the opinion of the last observer’s opinion was contrasting the other. Moreover it has been done a distinction between arterial and venous frequency content, in order to test a classification considering only one or both contents within the same image.

The results from newly divided data shown much more improvement especially in some subsets, however, these subsets contain a statistically small set of images, so are not idea for publication or medical application. Moreover confusion in classification could be due to sets having a combination of both high and low tortuosity vessels; future work may include plans to investigate the classification of single vessels.

CONCLUSIONS AND DISCUSSION

We have presented a novel characterization of the tortuosity of the whole retinal vasculature using spectral analysis, together with a novel measure of tortuosity. Theoretically the new method has three main desirable properties: it provides a rich and principled characterization of the bending frequency of a vessel; it is obtained directly, without arbitrary combinations of local, curvature-based measures: it leads to a natural measure of the tortuosity of the whole vasculature network.

The results have demonstrated a good reliability of the new technique for assessing single vessel tortuosity; while less positive outcomes have been gained from the classification test run in order to compare the measures of tortuosity obtained for vascular networks. This is probably due to unclear and uncertain annotations of the data set, in fact, better results have been achieved running tests with more defined annotations of the images.

Future works might involve, at first an investigation of the application of the method on synthetic data to ensure the algorithm works as expected on well-defined data; secondly the classification of images of the data sets should be reconsidered, since it has been proved to be highly affected by interpersonal subjectivity.

APPENDIX A: IMAGES CLASSIFICATION

A.1 CLASSIFICATION

The following table shows the classification of the images of the data set done by the three ophthalmologists (observe A, observe B and observer C). On the first column we find the number of the images, on the second one the class assigned by each observer for the images and on the third information about the overall agreement of the three doctors. Finally the on the last column it's indicated the class which the each image has been assigned to (1 for low tortuosity class, 2 for normal class, and 3 for high tortuosity class): each image has been assigned to a specific class when at least two observers agreed.

TABLE A.1: DATA SET

Images	*Observer A*	*Observer B*	*Observer C*	*All Same*	*2 Same*	*Different*	*GT class*
1	3	3	3	all same			3
2	2	2	2	all same			2
3	2	2	2	all same			2
8	3	3	1		2 same		3
44	3	3	3	all same			3
125	2	2	2	all same			2
128	2	2	2	all same			2
137	2	2	2	all same			2
173	1	1	2		2 same		1
209	2	2	2	all same			2
213	2	2	2	all same			2
273	2	2	2	all same			2
309	2	2	2	all same			2
312	2	2	2	all same			2
315	3	3	1		2 same		3
317	3	3	3	all same			3
325	1	1	1	all same			1
337	2	2	2	all same			2
368	3	3	3	all same			3
370	2	2	2	all same			2
379	2	2	2	all same			2

394	2	2	2	all same	2
404	1	1	3	2 same	1
405	3	3	3	all same	3
418	3	3	1	2 same	3
448	2	2	2	all same	2
451	2	2	2	all same	2
464	1	1	1	all same	1
519	1	1	1	all same	1
546	2	2	1	2 same	2
557	1	1	2	2 same	1
627	1	2	2	2 same	1
658	3	3	1	2 same	3
673	2	2	1	2 same	2
695	2	2	2	all same	2
698	2	2	2	all same	2
699	1	1	2	2 same	1
700	2	2	2	all same	2
730	2	2	2	all same	2
808	1	1	2	2 same	1
810	1	1	2	2 same	1
887	1	1	1	all same	1
896	1	1	1	all same	1
931	2	2	2	all same	2
952	2	2	2	all same	2
955	2	2	2	all same	2
959	2	2	2	all same	2
961	2	2	2	all same	2
1014	1	1	2	2 same	1
1017	1	1	1	all same	1
1055	1	1	1	all same	1
1057	1	1	1	all same	1
1061	3	3	1	2 same	3
1074	2	2	1	2 same	2
1111	2	2	2	all same	2
1113	2	2	2	all same	2
1182	1	1	2	2 same	1
1194	2	2	2	all same	2
1264	3	3	3	all same	3
1273	1	1	3	2 same	1

1276	1	1	2	2 same	1
1286	1	1	1	all same	1
1291	3	1	3	2 same	3
1323	1	3	2	all diff	excluded
1373	1	1	2	2 same	1
1376	1	1	2	2 same	1
1394	0	0	1	2 same	0
1396	1	1	1	all same	1
1411	2	2	2	all same	2
1413	2	2	2	all same	2
1416	2	2	2	all same	2
1419	2	2	2	all same	2
1439	2	2	2	all same	2
1474	2	2	2	all same	2
1495	2	2	2	all same	2
1497	2	2	2	all same	2
1507	3	3	1	2 same	3
1543	1	1	1	all same	1
1545	2	1	1	2 same	2
1557	1	1	2	2 same	1
1560	1	1	2	2 same	1
1648	2	2	2	all same	2
1677	1	1	2	2 same	1
1707	1	1	2	2 same	1
1722	2	2	2	all same	2
1725	2	2	2	all same	2
1734	1	1	2	2 same	1
1760	2	2	2	all same	2
1782	3	3	3	all same	3
1786	2	1	2	2 same	2
1815	2	2	2	all same	2
1864	1	1	1	all same	1
1866	1	1	1	all same	1
1900	1	1	1	all same	1
1942	3	3	3	all same	3
2024	2	2	2	all same	2
2027	2	2	2	all same	2
2031	2	1	2	2 same	2
2034	1	1	3	2 same	1

2035	2	2	2	all same	2
2041	1	1	2	2 same	1
2051	3	3	1	2 same	3
2084	3	1	3	2 same	3
2091	3	3	3	all same	3
2095	1	1	2	2 same	1
2098	2	2	2	all same	2
2123	1	1	1	all same	1
2132	3	3	1	2 same	3
2151	3	3	3	all same	3
2166	3	1	2	all diff	excluded
2237	3	3	3	all same	3
2293	2	2	2	all same	2
2392	1	1	2	2 same	1
2395	1	2	2	2 same	1
2437	1	1	2	2 same	1
2440	1	1	2	2 same	1
2477	2	2	2	all same	2
2480	3	3	3	all same	3
2553	2	2	2	all same	2
2619	2	2	2	all same	2
2625	2	2	2	all same	2
2683	2	2	2	all same	2
2685	2	2	2	all same	2
2687	2	2	2	all same	2
2688	1	1	2	2 same	1
2689	3	3	3	all same	3
2690	2	2	2	all same	2
2733	2	1	1	2 same	2
2767	3	3	3	all same	3
2768	3	1	3	2 same	3
2771	2	2	2	all same	2
2774	2	2	2	all same	2
2806	3	3	3	all same	3
2821	1	3	1	2 same	1
2840	2	2	2	all same	2
2842	2	2	2	all same	2
2848	1	1	1	all same	1
2912	2	1	2	2 same	2

2944	2	2	2	all same	2
2950	1	1	2	2 same	1
2951	1	1	2	2 same	1
2996	1	1	1	all same	1
2999	1	3	1	2 same	1
3011	2	2	2	all same	2
3023	2	2	2	all same	2
3026	1	1	2	2 same	1
3028	1	1	2	2 same	1
3206	1	1	2	2 same	1
3217	1	1	2	2 same	1
3299	2	2	2	all same	2
3302	2	2	2	all same	2
3409	2	2	2	all same	2
3423	2	2	2	all same	2
3425	2	2	2	all same	2
3429	2	2	2	all same	2
3430	2	2	2	all same	2
3449	2	2	2	all same	2
3458	1	1	2	2 same	1
3488	1	3	3	2 same	1
3526	1	1	1	all same	1
3671	2	2	2	all same	2
3672	2	2	2	all same	2
3688	2	2	2	all same	2
3690	2	2	2	all same	2
3699	2	2	2	all same	2
3721	2	2	2	all same	2
3722	2	2	2	all same	2
3725	1	1	2	2 same	1
3727	1	1	2	2 same	1
3792	2	2	2	all same	2
3869	2	2	2	all same	2
3904	2	2	2	all same	2
3907	2	2	2	all same	2
3965	1	1	2	2 same	1
3969	2	2	2	all same	2
3971	1	1	2	2 same	1
3973	2	2	2	all same	2

3976	2	2	1	2 same	2
3979	1	1	1	all same	1
4017	1	1	2	2 same	1
4063	1	1	2	2 same	1
4108	1	1	2	2 same	1
4208	1	1	2	2 same	1
4226	1	1	2	2 same	1
4284	1	1	1	all same	1
4380	1	1	1	all same	1
4382	1	1	1	all same	1
4392	2	2	2	all same	2
4394	2	2	2	all same	2
4399	1	1	1	all same	1
4407	2	2	2	all same	2
4423	0	0	2	2 same	0
4450	2	2	2	all same	2
4452	2	2	2	all same	2
4493	2	2	2	all same	2
4522	2	2	2	all same	2
4558	1	1	1	all same	1
4587	1	1	1	all same	1
4628	3	3	3	all same	3
4631	3	3	3	all same	3
4739	1	1	1	all same	1
4774	1	1	1	all same	1
4809	1	1	1	all same	1
4816	2	2	2	all same	2
4888	1	1	2	2 same	1
4893	1	1	2	2 same	1
4898	2	2	2	all same	2
4985	1	1	2	2 same	1
4987	1	1	1	all same	1
4989	2	2	2	all same	2
5009	3	3	1	2 same	3
5011	2	2	2	all same	2
5012	2	2	2	all same	2
5053	3	3	3	all same	3
5096	3	3	3	all same	3
5180	2	2	2	all same	2

5181	2	2	2	all same	2
5220	2	2	2	all same	2
5260	2	2	1	2 same	2
5314	2	2	2	all same	2
5315	2	2	2	all same	2
5381	2	1	2	2 same	2
5453	2	2	2	all same	2
5455	2	2	2	all same	2
5457	2	2	2	all same	2
5463	2	2	2	all same	2
5495	2	2	2	all same	2
5498	2	2	2	all same	2
5501	2	2	2	all same	2
5503	2	2	2	all same	2
5506	2	2	2	all same	2
5508	2	2	2	all same	2
5511	2	2	2	all same	2
5514	2	2	2	all same	2
5523	1	1	1	all same	1
5525	2	2	2	all same	2
5588	3	3	2	2 same	3
5590	1	1	2	2 same	1
5594	2	2	2	all same	2
5595	2	2	2	all same	2
5612	1	1	2	2 same	1
5615	1	1	2	2 same	1
5644	3	1	3	2 same	3
5649	1	1	3	2 same	1
5653	1	1	3	2 same	1
5685	1	1	1	all same	1
5689	3	3	3	all same	3
5722	3	3	3	all same	3
5749	1	1	1	all same	1
5756	2	2	2	all same	2
5757	3	1	1	2 same	3
5758	2	2	2	all same	2
5791	2	2	2	all same	2
5792	2	1	2	2 same	2
5799	2	2	2	all same	2

5818	2	2	2	all same	2
5836	3	3	3	all same	3
5902	1	1	1	all same	1
5904	1	1	2	2 same	1
5954	2	2	3	2 same	2
6022	2	2	2	all same	2
6025	2	2	2	all same	2
6062	3	3	1	2 same	3
6064	3	1	1	2 same	3
6066	1	1	1	all same	1
6131	2	2	2	all same	2
6211	2	2	2	all same	2
6213	2	2	2	all same	2
6242	3	3	3	all same	3
6309	2	2	2	all same	2
6316	2	2	2	all same	2
6323	2	2	2	all same	2
6325	2	2	2	all same	2
6366	2	2	1	2 same	2
6369	3	3	3	all same	3
6425	1	1	3	2 same	1
6433	2	2	2	all same	2
6500	3	3	3	all same	3
6627	1	1	1	all same	1
6677	2	2	2	all same	2
6680	2	2	2	all same	2
6688	1	1	1	all same	1
6696	1	1	1	all same	1
6722	2	1	2	2 same	2
6723	2	2	2	all same	2
6797	2	1	2	2 same	2
6800	1	1	1	all same	1
6833	2	2	2	all same	2
6835	2	2	2	all same	2
6962	2	1	1	2 same	2
7040	1	1	2	2 same	1
7045	1	1	2	2 same	1
7048	1	1	2	2 same	1
7091	1	1	2	2 same	1

7092	1	1	2	2 same	1
7125	2	2	1	2 same	2
7175	3	1	3	2 same	3
7176	1	1	1	all same	1
7192	2	2	2	all same	2
7236	1	1	3	2 same	1
7269	1	1	3	2 same	1
7270	1	1	3	2 same	1
7369	1	1	3	2 same	1
7370	1	2	1	2 same	1
7406	2	2	2	all same	2
7578	3	3	3	all same	3

A.2 IMAGES ANNOTATIONS

The following tables show the images selected within the data set with the annotation added by the fourth ophthalmologist. Column one and two show the number of the image and the class which the image has been assign to; on the third column the last ophthalmologist annotate his personal agreement with the previous classification, where 1 stands for clear classification and 2 stands for unclear classification. On the fourth column it has been highlighted which between arterial and venous component was the most relevant in each image. Finally on the last column the observer posted some notes indicating why, according to him, the classification is uncertain.

TABLE A.2: LOW CLASS ANNOTATION

img	***class***	***certain(1) or uncertain(2)***	***V (1) or A (2)***	***Notes***
519	1	1	1	
627	1	1	1	
887	1	1	1	
896	1	2	2	*Venous component is normal
1017	1	1	1	
1055	1	1	1	
1057	1	1	1	

1276	1	2	2	*Venous component is normal
1286	1	1	1	
1557	1	2	2	
1677	1	1	1	
1707	1	2	2	*Venous component is normal
1864	1	1	1	
2095	1	2	2	*Venous component is normal
2437	1	2	2	*Venous component is normal
2821	1	1	1	
2848	1	1	1	
2950	1	2	2	*Venous component is normal
2999	1	1	1	
3026	1	1	1	
3028	1	2	2	*Venous component is normal
3217	1	2	2	*Venous component is normal
3526	1	1	1	
3725	1	2	1	
3965	1	2	1	*Venous component is normal
3979	1	1	2	
4017	1	2	2	*Venous component is normal
4108	1	2	1	*Venous component is normal
4382	1	1	1	
4399	1	1	1	
4587	1	1	1	
4774	1	1	1	
4809	1	1	1	
4987	1	1	1	
5523	1	1	1	
5590	1	2	2	* Arterial component is low tortuous
5653	1	1	1	
5685	1	1	1	
5902	1	1	2	* Arterial component is low tortuous
5904	1	1	2	* Arterial component is low tortuous
7091	1	2	1	
7092	1	2	2	

TABLE A.3: NORMAL CLASS ANNOTATION

img	*class*	*certain(1) or uncertain(2)*	*V(1) or A (2)*	*Notes*
2	2	1	1	
3	2	1	1	
125	2	1	1	
128	2	1	1	
137	2	1	1	
213	2	1	1	
273	2	1	1	
370	2	1	1	
379	2	1	1	
730	2	1	1	
1074	2	1	1	
1113	2	1	1	
1413	2	1	1	
1439	2	1	1	
1474	2	1	1	
1648	2	1	1	
1725	2	1	1	
1815	2	1	1	
2035	2	1	1	
2685	2	1	1	
2690	2	2	1	
2771	2	1	1	
3302	2	1	1	
3976	2	2	1	* Arterial component is tortuous
4394	2	1	1	
4452	2	1	1	
4522	2	1	1	
5011	2	1	1	* Low arterial tortuosity
5012	2	2	1	* Low arterial tortuosity
5260	2	1	1	* Low arterial tortuosity
5457	2	1	1	
5498	2	2	1	
5503	2	1	1	
5514	2	1	1	

TABLE A.4: HIGH CLASS ANNOTATION

img	*class*	*certain(1) or uncertain(2)*	*V (1) or A (2)*	*Notes*
8	3	1	2	
317	3	1	1	
368	3	1	1	
405	3	1	1	
418	3	2	1	
1061	3	1	1	
1264	3	1	1	
1942	3	1	1	
2084	3	1	2	
2091	3	1	2	
2237	3	2	1	
2480	3	1	1	
2689	3	1	1	
2768	3	1	1	
2806	3	1	1	
4628	3	1	1	
4631	3	1	1	
5009	3	2	1	
5053	3	1	1	
5096	3	1	1	
5689	3	1	1	
5722	3	1	1	
6062	3	1	2	
6369	3	1	1	

A.3 Classification Tests: Confusion Matrices

In the section we decided to collect all the result of the last set of classification tests. Images have been divided considering the annotations of the four ophthalmologists and even if in some cases the results are good, the subsets contain a statistically small number of images so are not ideal for publication or medical application.

A.3.1 TESTS RUN ACCORDING TO THE FIRST ANNOTATIONS

Table A.5: test2_1, certain images, arteries only

		predicted classes		
		normal	low	high
actual classes	normal	6	5	9
	low	0	24	6
	high	0	2	15

Percent Results		**predicted classes**		
		normal	low	high
actual classes	normal	30	25.00	45.00
	low	0	80.00	20.00
	high	0	11.7647	88.2353

Table A.6: test2_2, certain images, veins only

		predicted classes		
		normal	low	high
actual classes	normal	9	10	1
	low	1	28	1
	high	5	5	7

Percent Results		**predicted classes**		
		normal	low	high
actual classes	normal	45.00	50.00	5.00
	low	3.3333	93.3333	3.3333
	high	29.4118	29.4118	41.1765

Table A.7: test2_3, certain images, arteries and veins

		predicted classes		
		normal	low	high
actual classes	normal	13	7	0
	low	2	28	0
	high	5	3	9

Percent Results		predicted classes		
		normal	low	high
actual classes	normal	60.0000	35.0000	0
	low	6.6667	93.3333	0
	high	29.4118	17.6471	52.9412

Table A.8: test2_4, uncertain images, arteries only

		predicted classes		
		normal	low	high
actual classes	normal	15	7	0
	low	0	4	0
	high	0	1	6

Percent Results		predicted classes		
		normal	low	high
actual classes	normal	68.1818	31.8182	0
	low	0	100.0000	0
	high	0	14.2857	85.7143

Table A.9: test2_5, uncertain images, veins only

		predicted classes		
		normal	low	high
actual classes	normal	15	1	6
	low	0	4	0
	high	0	0	7

Percent Results		**predicted classes**		
		normal	low	high
actual classes	normal	68.1818	4.5455	27.2727
	low	0	10.0000	0
	high	0	0	100.0000

Table A.10: test2_6, uncertain images, arteries and veins

		predicted classes		
		normal	low	high
actual classes	normal	13	2	7
	low	0	4	0
	high	0	0	7

Percent Results		**predicted classes**		
		normal	low	high
actual classes	normal	59.0909	9.0909	31.8182
	low	0	100.0000	0
	high	0	0	1000.0000

Table A.11: test2_7, certain and uncertain images, arteries only

		predicted classes		
		normal	low	high
actual classes	normal	12	18	12
	low	0	28	6
	high	0	7	17

Percent Results		**predicted classes**		
		normal	low	high
actual classes	normal	28.5714	42.8571	28.5714
	low	0	82.3529	17.6471
	high	0	29.1667	70.8333

Table A.12: test2_8, certain and uncertain images, veins only

		predicted classes		
		normal	low	high
actual classes	normal	19	20	3
	low	2	31	1
	high	2	12	10

Percent Results		**predicted classes**		
		normal	low	high
actual classes	normal	45.2381	47.6190	7.1429
	low	5.8824	91.1765	2.9412
	high	8.3333	50.0000	41.6667

A.3.2 TEST ACCORDING TO LAST OBSERVER ANNOTATIONS

Table A.13: test1_1, certain images, arteries only

		predicted classes		
		normal	low	high
actual classes	normal	8	8	10
	low	0	25	4
	high	0	6	15

Percent Results		**predicted classes**		
		normal	low	high
actual classes	normal	30.7692	30.7692	38.4615
	low	0	86.2069	13.7931
	high	0	28.5714	71.4286

Table A.14: test1_2, certain images, veins only

		predicted classes		
		normal	low	high
actual classes	normal	12	13	1
	low	1	28	0
	high	4	8	9

Percent Results		**predicted classes**		
		normal	low	high
actual classes	normal	46.1538	50.0000	3.8462
	low	3.4483	96.5517	0
	high	19.0476	38.0952	42.8571

Table A.15: test1_3, certain images, arteries and veins

		predicted classes		
		normal	low	high
actual classes	normal	11	13	2
	low	2	26	1
	high	6	5	10

Percent Results		**predicted classes**		
		normal	low	high
actual classes	normal	42.3077	50.0000	7.6923
	low	6.8966	89.6552	3.4483
	high	28.5714	23.8095	47.6190

Table A.16: test1_4, uncertain images, arteries only

		predicted classes		
		normal	low	high
actual classes	normal	15	1	0
	low	0	5	0
	high	0	0	3

Percent Results		**predicted classes**		
		Normal	low	high
actual classes	normal	93.7500	6.2500	0
	low	0	100.0000	0
	high	0	0	100.0000

Table A.17: test1_5, uncertain images, veins only

		predicted classes		
		normal	low	high
actual classes	normal	14	2	0
	low	0	5	0
	high	0	0	3

Percent Results		**predicted classes**		
		normal	low	high
actual classes	normal	87.5000	12.5000	0
	low	0	100.0000	0
	high	0	0	100.0000

Table A.18: test1_6, uncertain images, arteries and veins

Percent Results		**predicted classes**		
		normal	low	high
actual classes	normal	16	0	0
	low	0	5	0
	high	0	0	3

Percent Results		**predicted classes**		
		normal	low	high
actual classes	normal	100,0000	0	0
	low	0	100,0000	0
	high	0	0	100,0000

Table A.19: test1_7, certain and uncertain images, arteries only

Percent Results		predicted classes		
		normal	low	high
actual classes	normal	12	18	12
	low	0	28	6
	high	0	7	17

Percent Results		predicted classes		
		normal	low	high
actual classes	normal	28.5714	42.8571	28.5714
	low	0	82.3529	17.6471
	high	0	29.1667	70.8333

Table A.20: test1_8, certain and uncertain images, veins only

Percent Results		predicted classes		
		normal	low	high
actual classes	normal	19	20	3
	low	2	31	1
	high	2	12	10

Percent Results		predicted classes		
		normal	low	high
actual classes	normal	45.2381	47.6190	7.1429
	low	5.8824	91.1765	2.9412
	high	8.3333	50.0000	41.6667

APPENDIX B: BACKGROUND STUDIES

PRINCIPAL COMPONENT ANALYSIS, PCA

PCA is mathematically defined as an orthogonal linear transformation that transforms the data into a new coordinate system such that the greatest variance by any projection of the data comes to lie on the first coordinate, called first principal component. In a multidimensional space the first principal component is the direction in the feature space along which projections have the largest variance. The second principal component is the direction which maximizes the variance among all directions orthogonal to the first.

COMPUTATIONAL PART

Given a data matrix with *p* variables and *n* samples, the data are first centered on the means of each variable. This will ensure that the features are centered on the origin of the principal component, but do not affect the spatial relationship of the data nor the variances along the variables. The first principal component (Y_1) is given as the linear combination of the variables $X_1, X_2, \ldots, X_p$:

$$Y_1 = a_{11} \cdot X_1 + a_{12} \cdot X_2 + \cdots + a_{1p} \cdot X_p$$

or, in a matrix notation

$$Y_1 = a_1^T \cdot X$$

The first principal component is calculated such that it accounts for the greatest possible variance in the data set, and the coefficients of the linear combination are calculated with the constraint that their sum of squares is 1

$$a_{11}^2 + a_{12}^2 + \cdots + a_{1p}^2 = 1$$

The second principal component is calculated in the same way, with the condition that it is uncorrelated with (i.e. perpendicular to) the first principal component and that it accounts for the next highest variance.

$$Y_2 = a_{21} \cdot X_1 + a_{22} \cdot X_2 + \cdots + a_{2p} \cdot X_p$$

This continues until a total of *p* principal components have been calculated, equal to the original number of variables. At this point, the sum of the variances of all the principal components will equal the sum of the variance of all the variables, that is, all of the original information has been explained or accounted for. Collectively, all these transformation of the original variables to the principal components is

$$Y = X \cdot A$$

The rows of the matrix A are called the eigenvectors of matrix Sx, the variance-covariance matrix of the original data. The elements in the diagonal of matrix Sy, variance-covariance of the principal components, are known as the eigenvalues. Eigenvalues are the variance explained by each principal component and are constrained to decrease monotonically form the first principal components to the last.

MATLAB IMPLEMENTATION

We implemented a function, *functionPCA*, which computes the PCA of the centerline of the vessel to be rotated: the pixels that describe the vessel centerline are the input parameters of the function.

```
function vessPostPCA = functionPCA(vessIn)
% ---------- ReMap Vessel to PCA axes
    % Find main elongation direction, d, and rotate axes so that x
axis is
    % aligned with d.
    % this tries to avoid that the vessel points are not 1-to-1
function.

    numPixInVes = length(vessIn);

    % centre of gravity (baricentrum)
    vesCoG = [mean(vessIn(:,1)),mean(vessIn(:,2))];
    vesCoG = vesCoG'; % transpose --> column vector


    vesInXl = vessIn - ones(numPixInVes,1)*vesCoG';
    autocorr = vesInXl'*vesInXl;
    [V, D] = eig(autocorr); %  eigenvalues (V) and eigenvectors (D)


    vessPostPCA = vessIn*flipdim(V,2); % rotate, keep centered in
the origin
```

The length of the vessel and the origin of the principal components are estimate (*vesCoG*); then the vessel is centered in the origin (*vesInXl*) and the variance-covariance matrix is calculated (*autocorr*). From the variance-covariance matrix the eignevalues and the eigenvectors are extracted; finally the input centerline is rotate according to the direction highlighted by the eigenvectors.

REFERENCES

[1] A.C. Delgado, C.T. Brandt, F. Venture, F. Oréfice "Retinal Fluorescein Contrast Arrival Time of Young Patients with the Hepatosplenic From of the Schistosomiasis Mansoni", *Mem Inst Oswaldo Cruz*, Vol. 97(Suppl.1): 161-164, 2002

[2] M.D. Abràmoff, M.K. Garvin, M. Sonka "Retinal Imaging and Image Analysis", *IEEE Reviews in Biomedical Engineering*, vol.3, 2010

[3] A. Perez-Rovira, T. MacGillivray, E.Trucco, K.S. Chin, K. Zutis, C. Lupascu, D. Tegolo, A. Giacchetti, P.J. Wilson, A. Doney and B. Dhillon "VAMPIRE : Vessel Assessment and Measurement Platform for Images of the REtina"

[4] A. Ruggeri, E. Poletti, D. Fiorin, L. Tramontin "From laboratory to clinic: the development of web-based tools for the estimation of retinal diagnostic parameters", *Conf Proc IEEE Eng Med Biol Soc*, 2011

[5] D. Fiorin, A. Ruggeri "Computerized Analysis of Narrow-fiel ROP Images for the Assessment of Vessel Caliber and Tortuosity", *Con Proc IEEE Eng Med Biol Soc.*, 2011

[6] C.S. Cheung, Z. Butty, N.N. Tehrani, W.C. Lam "Computer-assisted Image Analysis of Temporal Retinal Vessel Width and Tortuosity in Retinopathy of Prematurity for the Assessment of Disease Severity and Treatment Outcome", *J AAPOS*, 2011

[7] M.T. Cabrera, S.F. Freedman, A.E. Kiely, M.F. Chiang, D.K. Wallace "Combining ROPtool Measurements of Vascular Tortuosity and Width to Quantify Plus Disease in Retinopaty of Prematurity", *J AAPOS*, 2011

[8] C.Y. Cheung, Y. Zheng, W. Hsu, M.L. Lee, Q.P. Lau, P. Mithcell, J.J. Wang, R. Klein, T.Y. Wong "Retinal Vascular Tortuosity, Blood Pressure, and Cardiovascular Risk Factors", *Ophthalmolology*, 2011

[9] M.B. Sasongko, T.Y. Wong, T.T. Nguyen, C.Y. Cheung, J.E. Shaw, J.J. Wang "Retinal Vascular Tortuosity in Person with Diabetes and Diabetic Retinopathy", *Diabetologia*, 2011

[10] L. Hathout, H.M. Do "Vascular Tortuosity: a Mathematical Modeling Prospective", *J Physiol Sci*, 2012

[11] E. Trucco, H. Azegrouz, B. Dhillon "Modeling the Tortuosity of Retinal Vessels: Does Caliber Play a Role?", *IEEE Trans Biomed Eng*, 2010

[12] A. Bhuiyan, B. Nath, K. Ramamohanarao, R. Kawasaki, T.Y. Wong "Automated analysis of Retinal Vascular Tortuosity on Color Retinal Images", *J Med Syst*, 2012

[13] W.E. Hart, M. GoldBaum, B. Côté, P. Kube, M.R. Nelson "Measurement and Classification of Retinal Vascular Tortuosity", *Int J Med Inform*, 1999

[14] Z. Martin Rodriguez, P. Kenny, L. Gaynor "Improved Characterization of Aortic Tortuosity", *Med Eng Phys*, 2011